UNIVERSITY OF CALIFORNIA, SAN DIEGO

Unraveling the changes of extracellular matrix with age and fibrotic pathology

A Thesis submitted in partial satisfaction of the
requirements for the degree Master of Science

in

Bioengineering

by

Yun Xie

Committee in charge:

Professor Shyni Varghese, Chair
Professor Pedro Cabrales
Professor Michael Heller

2013

The thesis of Yun Xie is approved and it is acceptable in quality and form for publication on microfilm and electronically:

_____

_____

_____

Chair

University of California, San Diego

2013

TABLE OF CONTENTS

LIST OF FIGURES

ACKNOWLEDGEMENTS

First of all, I would like to give my sincere gratitude and appreciation to one of the most respectful people in my life, my committee chair, Professor Shyni Varghese. From being someone who knew minimal about the field and lab to someone who can handle experiments independently and help other people at the same time, I received numerous help from her. I want to thank Professor Varghese for her continuous support, trust, and guidance in my graduate study here at UCSD.

Next, I want to thank Professor Pedros Cabrales and Professor Michael Heller for being my committee members and taking time to give me suggestions and feedbacks for my graduate work.

During the past two years, not only I have grown academically, but also I have always been supported and loved by my lab members. They were my coworkers but at the same time loving and precious friends who shared my laughter and pulled me through these tough times. Specifically, I would like to thank Joshua, Manando, and Ruvi for their tremendous help in this project. I also want to express my appreciation for everyone else in my lab, Fei, Tuan-lin, Mrityunjoy, Aereas, Han, Young, Jacob, Cai, Harsha, Gus, Shruti, Heemin, Lynn, Thomas, Sam, Ameya, and Vernon. Without them, I would not be able to conquer all the obstacles I had in my sailing journey.

Last but not least, I would like to give my sincere appreciation to my parents and friends both at UCSD and from UCLA. Because of their continuous support, I was able to move forward; because of their continuous love, I did not give up in the middle. I truly appreciate for all these people who made impact in my life.

Chapter 2, in full, is currently being prepared for submission for publication of the material: Xie, Yun; Chauhan, Ruvi; Hwang, Yongsung; Lin, Susan; Seo, Timothy; Varghese, Shyni. The thesis author was the primary investigator and author of this paper.

Chapter 3, in part, will be prepared for submission for publication of the material: Nakasaki, Manando; Hwang, Yongsung; Xie, Yun; Varghese, Shyni; Jamora, Colin. The thesis author will be the co-author of this paper.

ABSTRACT OF THE THESIS

Unraveling the changes of extracellular matrix with age and fibrotic pathology

by

Yun Xie

Master of Science in Bioengineering

University of California, San Diego, 2013

Professor Shyni Varghese, Chair

Extracellular matrix (ECM) is a dynamic scaffold that provides both structural support and functional integrity to various tissues and organs. By serving as a natural reservoir to a variety of resident cells, ECM actively interacts with these residing cells and regulates their behaviors ranging from differentiation and proliferation to migration and regeneration. Due to its dynamic nature, ECM constantly undergoes remodeling as the local tissues experience either physiological or pathological changes, such as aging and fibrosis. Therefore, understanding the changes occur in ECM may

help the development of clinically translated stem cell applications for conditions like aging and fibrosis.

In this thesis, we examine the changes that ECM undergoes with aging and pathogenesis by using two different organ systems, skeletal muscles and skin. Specifically, in the first study, we determine the biochemical changes of ECM in muscles of both wild type and dystrophic mice at various ages. We also demonstrate the structural changes of ECM associated with aging and muscle pathology. In the second study, we establish a decellularized skin model to study the effect of extracellular matrix on fibroblast behavior in an effort to understand the role of ECM on fibrosis progression. Our results show that aging and disease have a tremendous effect on biochemical composition of ECM in skeletal muscles. Also, we demonstrate that the decellularized skin model has the potential of studying the role of ECM properties on skin fibrosis, and decellularized tissue has an effect on activation of fibroblasts.

CHAPTER 1: INTRODUCTION

1.1) Motivation and background

1.1.1) Extracellular matrix and its components

Extracellular matrix or ECM is a biological scaffold with a meshwork structure that provides both structural and functional integrity to various organs. It constantly experiences remodeling in response to environmental changes, thus giving its dynamic nature. ECM also serves as a natural cell reservoir, which resides millions of different cells and at the same regulate their behaviors, such as proliferation, differentiation, migration, regeneration, and degeneration [1]. Besides storing various growth factors, providing tissues with proper structure, and transducing mechanical signals, ECM, in addition, functions as an adhesive substrate and presents receptors to their growth factors (Fig. 1) [2].

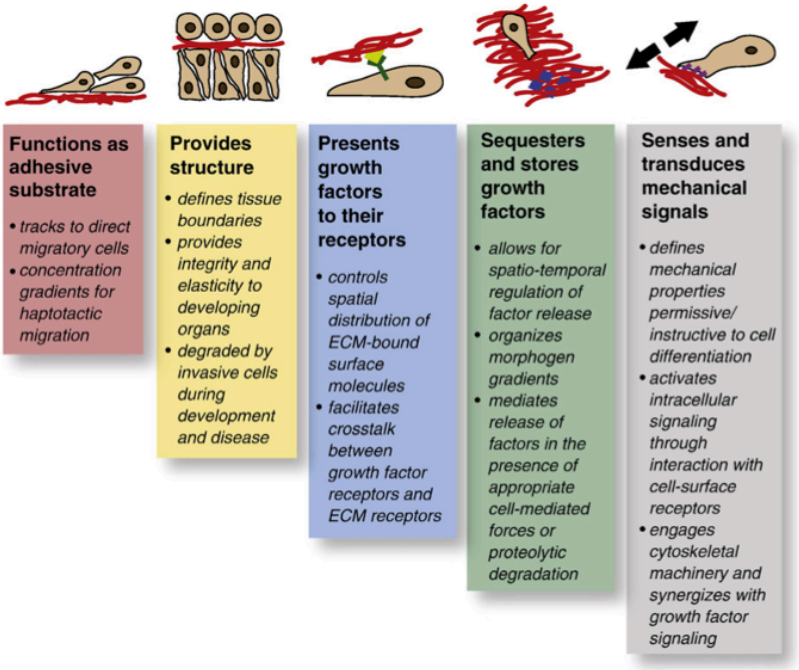

Figure 1. Summary of ECM functions.
Adapted from [2].

ECM in tissues consists of two major components: structure proteins and proteoglycans. Depending on different organs and tissues, composition of these components tends to vary [3]. Structure protein, as what its name states, can provide mechanical properties to the tissues. Some of the structure proteins commonly found in ECM are collagen, elastin, and fibronectin [1]. Collagen, the most abundant protein in ECM, may constitute up to about 30% of total protein content in mammals. With its unique triple-helical structure, collagen provides mechanical support, maintains structural integrity, and contributes to tissue organization and shape in both developing and later stages [4, 5]. Elastin is another structure protein that is abundant in connective tissues like skin and ligament and typically serves to provide tissue elasticity. Elastic fibers also contribute to the mediation of cell attachment and the regulation of TGF-β [6]. The third major structure protein is fibronectin, which like other types of protein in this category, acts as a mechano-regulator and mediates cell attachment [7]. In addition, studies have found that fibronectin is actively involved in the wound healing by forming blood clot with fibrin at injury site [8].

The second major component of ECM is proteoglycan, typically consisted of a core protein covalently linked with a glycosaminoglycan (GAG) chain with an exception of hyaluronan (HA), which lacks of a core protein [9]. Current classification divides proteoglycans into three major categories: small leucin-rich proteoglycans (SLRPs), modular proteoglycans, and cell-surface proteoglycans [10]. Although each type of proteoglycans has specific functions, all proteoglycans play a crucial role in various cellular processes and signaling pathways [9-11]. Also, there are other cellular

components, such as growth factors, integrin-binding receptors, and proteolytic enzymes, which continuously interact with the ECM network in a number of cell signaling transductions [12-14].

1.1.2) ECM and aging

Due to its dynamic nature, ECM can undergo remodeling during various physiological and pathological conditions, such as aging and fibrosis. Aging is considered a physiological condition associated with many micro-environmental changes. Among them, increased fibrous connective tissue and decreased regenerative capacity are the two major changes related to aging [15]. Previously, Rando and his colleagues have demonstrated the influence of systemic factors on age-related decline in muscle progenitor cells. In this study, when the aged progenitor cells were exposed to serum of young animals, such decline in regenerative ability was rescued [16]. These findings directly suggest that the micro-environment and niche that the progenitor cells reside can play a crucial role in the process of aging.

1.1.3) ECM and fibrosis

During a normal wound healing process, following tissue injury, activated platelets first migrate to the injury site for blood clot formation. This is followed by recruitment of inflammatory cells upon release of growth factors, chemokines, and cytokines by local epithelial or endothelial cells. Activated macrophages and neutrophils travel to the damaged tissue and engulf dead cells, foreign substances, and tissue debris [17, 18]. These leukocytes at the same time produce cytokines like IL-13 and TGF-β, which activates resident fibroblasts and more macrophages [19, 20]. The

activated fibroblasts or myofibroblasts produce new ECM components at the injury site while endothelial cells form new blood vessels. After newly produced collagen fibrils become more organized, endothelial and epithelial cells begin restoration of basal layers to complete formation of new endothelium and epithelium, which in turn concludes the normal wound healing process [21]. However, when the injury becomes chronic, persistent inflammation and activation of fibroblasts may take place, leading to a non-physiological scarring process termed fibrosis (Fig. 2) [18].

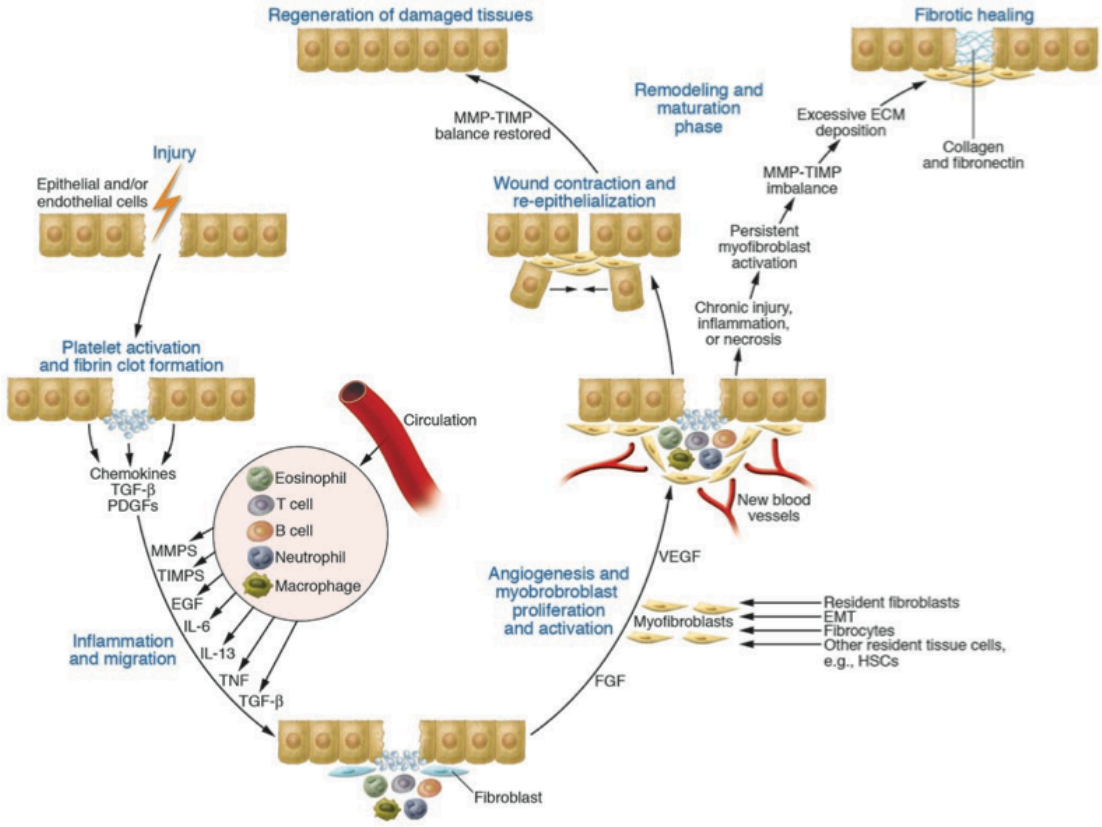

Figure 2. Overview of wound healing and fibrotic cascade.
Adapted from [18].

1.1.3.1) Fibrosis and its role in different organs

Fibrosis is defined as a pathological tissue repair process typically associated with excessive deposition of extracellular matrix and chronic loss of many organ functions, ultimately leading to organ dysfunction [18, 22]. Fibrosis plays a crucial role in the progression of many chronic diseases in organs like skin, liver, heart, kidney, lung, skeletal muscle, and so on [22]. Some common features of different tissue fibrosis include excessive accumulation of ECM leading to tissue stiffness, paleness resulting from rarefication of the vasculature, and uneven surfaces reflecting constant fibroblast contraction (Fig. 3) [22].

Fibrosis in skin varies from hypertrophic scars to scleroderma to keloids. Unlike other localized fibrotic lesions, skin fibrosis can lead to systemic sclerosis, affecting not only skin, but also other internal organs such as lung and heart [23, 24]. In liver, fibrosis is typically caused by viral hepatitis, alcohol-induced, and non-alcoholic steatopepatitis. One of the most clinically relevant tissue fibrosis occurs in liver, called Cirrhosis, which results from chronic liver disease characterized by replacement of liver tissue with fibrotic scar tissues, leading to dysfunction of liver [25]. Cardiac fibrosis associated with an abnormal thickening of heart valves or wall is generally induced various heart diseases, such as hypertension, coronary artery diseases, and aortic stenosis [26, 27]. Renal fibrosis, which can occur in diseases like Diabetes Mellitus, hypertension, and glomerulonephritis, is typically associated with an excessive deposition of ECM in renal parenchyma, causing progressive glomerulosclerosis and ultimately leading to loss of organ function [28]. Fibrosis of

lung, primarily associated with restricted ventilators, is generally associated with most chronic lung pathologies like idiopathic pulmonary diseases, emphysema, and sarcoidosis. Unlike fibrosis in other organs, relatively mild fibrotic lesions may lead to detrimental effects [29]. Fibrosis in skeletal muscles is rather apparent in most muscular dystrophies. Like fibrosis in other tissues, fibrosis in muscular dystrophies is generally associated with excessive accumulation of ECM, leading to substitution of muscle fibers with fibrotic connective tissues [30, 31].

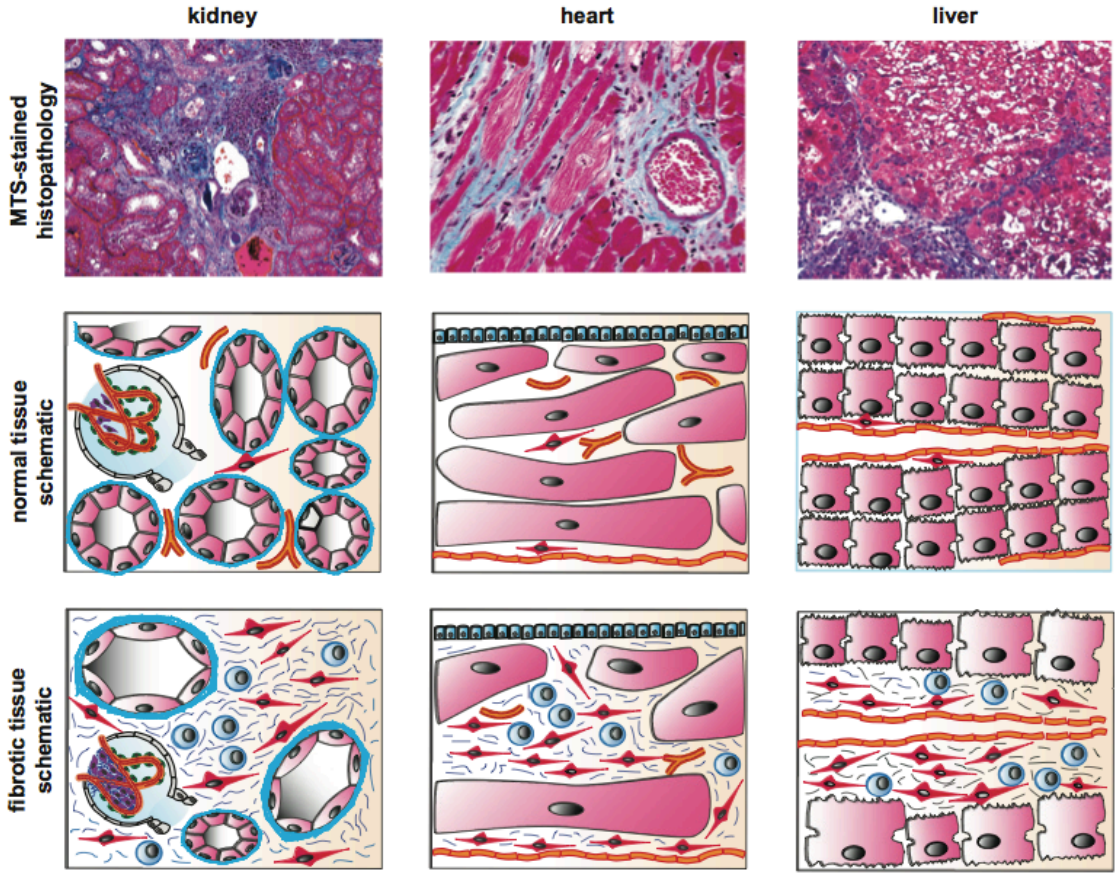

Figure 3. Common features of tissue fibrosis.
Adapted from [22].

1.1.3.2) Fibrosis and its mechanisms

In fibrosis, activated fibroblasts are considered as one of the key cellular mediators [32, 33]. Activated fibroblasts, also referred to as myofibroblasts, are contractile cells specifically expressing α-smooth muscle actin [34]. In normal wound healing, myofibroblasts actively participate in repair and regeneration of the tissue and undergo apoptosis after re-epithelialization of the wound. However, myofibroblasts in fibrotic state are resistant to the programmed death [17]. They are constantly under activated state and produce excessive amount of connective tissue. Originally, activated fibroblasts are thought to be derived solely from resident mesenchymal fibroblasts [18]. Recent findings suggest that there are additional sources contributing to the population of activated fibroblasts in fibrosis. Epithelial cells and endothelial cells can convert to myofibroblasts through the process of epithelial-mesenchymal-transition (EMT) and endothelial-mesenchymal-transition (EnMT) respectively [35-37]. Bone marrow-derived fibrocytes can contribute to the fibroblast accumulation. In fact, back in 1990s, Bucala *et al* have identified this circulating population of cells and established its role in tissue repair [38, 39]. Furthermore, vascular smooth muscle cells and pericytes have been reported to build up the population of the connective tissue fibroblasts in fibrogenesis [40].

Since myofibroblast is a key mediator in fibrosis, many studies have been conducted to understand the underlying mechanisms regulating fibroblast activation. Activation, proliferation, migration, and survival of fibroblasts are regulated either directly or indirectly by a number of different soluble and insoluble factors and

physical changes in the environment. These factors include cytokines such as IL-13 and TGF-β, growth factors such as connective tissue growth factor (CTGF) and platelet-derived growth factor (PDGF), and ECM properties such as stiffness [17]. A summary of different origins of myofibroblasts and mediators for activation of fibroblasts is shown in Fig. 4.

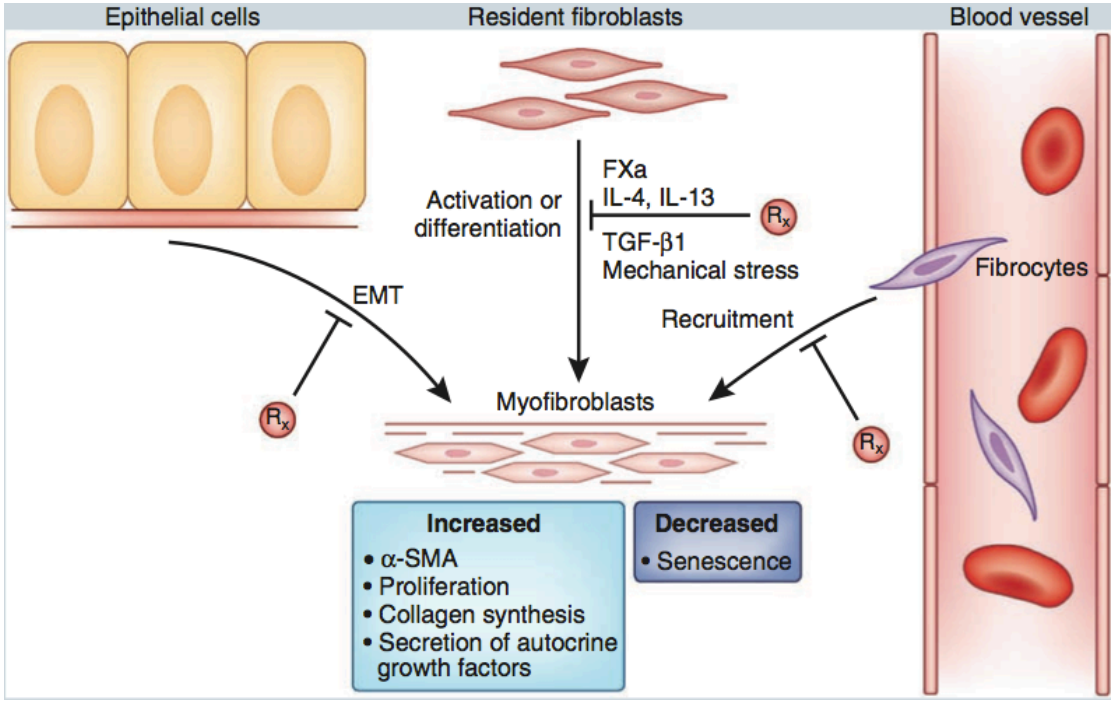

Figure 4. Origin of myofibroblasts.
Adapted from [17].

1.1.3.3) Cytokines

Interleukin-13 or IL-13 is a CD4+ T helper cell associated cytokine. A number of studies have demonstrated the dominant role of IL-13 in the development of lung and skin fibrosis [41, 42]. In fibrotic tissues, IL-13 can induce fibrosis both directly and indirectly. Lee *et al* has found that IL-13 stimulates the production and activation of TGF-β, which in turns activates local quiescent fibroblasts [43]. However,

Kaviratne *et al* has shown that activation of fibrosis by IL-13 is independent of TGF-β [44]. On the other hand, transforming growth factor-β or TGF-β has always been known for its profibrotic activities in many chronic organ fibrosis. Like IL-13, TGF-β is also secreted by lymphocytes during the initial phase of inflammation [19]. Besides the predominate role in activation of fibroblasts, TGF-β is also involved in the stimulation of protease inhibitors that are responsible for breakdown of ECM [45].

1.1.3.4) Growth factors

Platelet-derived growth factors (PDGFs) are predominantly in the promotion of myofibroblasts proliferation and survival. During initial phase of tissue repair, PDGFs are secreted by a variety of cell types in response to injury, which in turns attracts local myofibroblasts through production of different mediators [46]. Connective tissue growth factors (CTGFs), on the other hand, share many similarities with PDGFs. The presence of CTGF in fibrotic diseases can be dated as early as in the 1990s in which an overexpression of this protein was found in skin fibrosis [47]. In addition, it has been identified that there is a cross-talk between TGF-β and CTGF with CTGF induced by TGF-β in, but at the same time working together to sustain fibrotic response [48].

1.1.3.5) Matrix factors

In fibrosis, tissue stiffness is a predominant pathological feature that results from progressive accumulation of collagen fibers, leading to changes of mechanical properties of tissue. However, recent studies have shown that such resulting mechanical alternation can in turn provide local cells with an altered environment that

favors further activation of resident fibroblasts and production of ECM and exacerbates this diseased state [49]. In addition, Wipff *et al* has demonstrated that in a stiff microenvironment, TGF-β, one of the predominant mediators of fibroblast activation, can be activated by the contractile forces generated by α-SMA expressing myofibroblasts [50].

1.2) Thesis objective

The aim of this thesis is to understand the changes that the extracellular matrix undergoes with aging and in fibrotic pathology and how these changes contribute to fibrosis. Specifically, I will study two organs/tissues, skeletal muscle and skin. In the first part of the thesis, I focus on determining the changes that the ECM experiences with aging and muscle wasting diseases like Duchenne muscular dystrophy (DMD). A characteristic feature of DMD is muscle fibrosis with disease progression. Second part of the thesis focuses on understanding the role of ECM properties on sustained activation of fibroblasts in tissue fibrosis. Here, we use skin fibrosis as a model system due to its availability and the *in vivo* model available without the presence of other pathological complications.

The following studies were performed to investigate skeletal muscle ECM with respect to age and muscle pathology:

1. Assess the changes in biochemical composition in different age groups of normal healthy and dystrophic skeletal muscles.
2. Study the morphological and structural changes in different muscle groups.

The following studies were performed to explore the impact of ECM physical properties on fibroblasts activation:

1. Establish a decellularization method that will maintain the biochemical compositions of the tissue.
2. Characterize the decellularized skin to determine its composition of ECM as compared to control skin.
3. Establish a cell culture system.
4. Assess the effect of ECM properties on fibroblast behavior through analysis of gene expression level of fibrosis-related genes.

1.3) Experimental setup

To investigate the changes in skeletal muscle ECM as a function of age and muscle pathology, four different ages of wild type mice were chosen: 3wk, 2mo, 6mo, and 11mo, along with three different ages of *mdx* mice, 3wk, 2mo, and 9mo. Specifically, we performed different biochemical assays on extensor digitorum longus (EDL), tibialis anterior (TA), and quadriceps (QUAD) to quantify the changes in ECM components, such as collagen and proteoglycan, and cellular components through total DNA content. We also histologically analyzed the TA muscles to evaluate the morphological changes. Lastly, we performed scanning electron microscope (SEM) analysis to evaluate the micro-structural changes of skeletal muscles.

To explore the impact of the physical properties of the skin on activation of fibroblasts, we used a wild type control, a fibrotic skin model (Snail transgenic mice), hereafter termed as fibrotic skin, and a Snail transgenic mouse treated to abolish

fibrosis pathology, hereafter termed as treated fibrotic skin. We developed a decellularization method to remove cellular components in the skin while maintaining the ECM components intact. In the second part of this study, we cultured primary dermal fibroblasts on the decellularized skin tissues for three and seven days to evaluate the expression level of fibrosis-related genes.

1.4) Summary of results

The above experiments led to the following results:

1. ECM component of skeletal muscle, such as collagen, increases with aging and *mdx* pathology while GAG and cellular components represented by total DNA content decrease with aging and muscle pathology.
2. Cross-sectional areas of muscle fibers tend to increase with aging, and while comparing between normal and dystrophic mice, *mdx* mice tend to have larger muscle fibers.
3. Isolated skin tissues can be successfully decellularized leaving majority of ECM components intact.
4. The fibroblasts cultured on decellularized fibrotic skin show higher levels of collagen type I expression compared to that of wild type skin.
5. Fibroblasts cultured on treated fibrotic decellularized skin show significant down-regulation of collagen type I. However, no such effects were observed in other fibrosis markers like α-SMA.

CHAPTER 2: SKELETAL MUSCLE EXTRACELLULAR MATRIX: EFFECT OF AGE AND PATHOLOGY

2.1) Introduction

Extracellular matrix (ECM) has a complex and dynamic structure that provides a scaffolding matrix for regulation of cellular behaviors and tissue regeneration [51]. The skeletal muscle ECM mainly consists of collagen, proteoglycans, and other cellular components [52, 53]. These well-orchestrated components play a significant role in maintaining the unique structural, compositional, and mechanical properties of the skeletal muscle. Moreover, the ECM of skeletal muscle is not only capable of transmitting extracellular force, maintaining skeletal muscle functions, but also serving as a biological reservoir for growth factors and regulating the functions of residing skeletal muscle stem cells [52]. Amongst various ECMs present in skeletal muscle, collagen, one of the most abundant proteins in the skeletal muscle, has been shown to provide important functions in muscle tensile strength and elasticity as well as in regulation of cell differentiation and attachment [54]. Proteoglycans, another major components of skeletal muscle, have been known for their active involvement in the development, differentiation, and regeneration of skeletal muscle [52, 55-57]. Numerous reports have demonstrated that these two important ECM proteins are highly associated with physiological aging as well as skeletal muscle diseases such as muscular dystrophies [58, 59]. Therefore, there has been an increasing surge of interests in understanding the roles of these two extracellular matrix proteins in skeletal muscle aging and muscle pathology.

Aging in skeletal muscle has been one of the most devastating physiological conditions for elders. In senior citizens, aging-related disorders do not only affect their overall life quality but may also lead to disability. In aging, muscles are predominantly replaced with excessive accumulation of ECM, mainly collagens, around the skeletal muscle fibers (fibrosis), resulting in the loss of muscle mass and muscle strength [60]. Moreover, it has been found that the regenerative capacity of skeletal muscles declines with aging [61]. Recently, Conboy and her colleagues have extensively demonstrated the critical roles of age-associated micro-environmental cues in regulating the skeletal muscle regeneration [57, 62]. Several studies have shown that exposure of older muscles to a younger environment may help restore a substantial regenerative ability [15, 16, 63]. All these findings suggest that the surrounding ECM plays a crucial role in the aging of skeletal muscles.

Besides aging, muscular dystrophies are another catastrophic diseases accompanied by muscle wasting. One severe form of muscular dystrophies is Duchenne Muscular Dystrophy (DMD), which is a X-linked genetic disorder caused by a mutation in the gene coded for a protein called dystrophin [64]. DMD patients generally suffer from severe fibrosis and inflammation in muscles [65]. Also, as the disease progresses, muscle fibers constantly undergo degeneration and regeneration [30, 66]. Consequently, there is an accumulated collagen deposition, ultimately progressing to fibrosis [67, 68]. In addition to those pathological changes, there are numerous changes on cellular basis, contributing to the devastating consequences of DMD.

In this study, we try to determine the age- and fibrotic pathology-associated biochemical changes of ECM and their underlying impact on the regulation of skeletal muscle functions and regeneration using wild type and dystrophic mice with a systematic increase in age.

2.2) Materials and Methods

2.2.1) Animal handling

All animal handling and experiments were carried out in accordance with the protocols approved by the UCSD Institutional Animal Care and Use Committee (IACUC) and NIH guidelines for animal welfare. To evaluate the effect of aging on biochemical compositions of skeletal muscle extracellular matrix (ECM), 3-week-old, 2-month-old, 6-month-old, and 11-month-old C57BL/10J mice were either bred and raised in lab's vivarium or purchased from the Jackson Laboratory. To further elucidate the effect of muscle pathology on biochemical compositions of skeletal muscle ECM, 3-week-old, 2-month-old, and 9-month-old C57BL/10ScSn-Dmd^{mdx}/J mice were purchased from the Jackson Laboratory and raised in lab's vivarium. Prior to isolation of skeletal muscles, all mice were euthanized by carbon dioxide and sacrificed through cervical dislocation. All extensor digitorum longus (EDL), tibialis anterior (TA), and quadriceps (QUAD) muscles were then harvested. All biochemical analysis was performed as biological triplicates.

2.2.2) Biochemical assays

2.2.2.1) Tissue preparation

Biochemical assays were performed on EDL, TA, and QUAD muscles from C57BL/10J wild type (WT) and C57BL/10ScSn-Dmd^{mdx}/J (*mdx*) mice as a function of age and DMD pathology. Isolated muscle samples were placed in clean pre-weighed empty 1.5mL Eppendorf tubes that were previously labeled and snap-frozen in liquid nitrogen. Tissues were stored at -80°C or lyophilized for 1-2 days directly. All dried samples were weighed to obtain dry weights of tissues.

2.2.2.2) Papain digestion

Dried muscles were digested with papain solution containing sterile papain and L-cysteine dissolved in PBE buffer. PBE buffer was prepared by dissolving 7.1g Na_2HPO_4 and 1.86g Na_2EDTA in 500mL dH_2O. pH was adjusted to 6.5 using concentrated HCl. The buffer was then filter-sterilized and stored at 4°C for future use. For making papainase, 24.2g L-cysteine with formula weight of 121.16g/mol was first dissolved in 20mL of pre-made PBE buffer. The solution was then filter-sterilized. 0.10mL of sterile papain stock was added to this solution via TB syringe and needle. Tissue samples were grinded into pieces with pellet pestle after 1mL of prepared papainase was added to each sample. Fully homogenized samples were placed in water bath at 60°C for at least 16 hours.

2.2.2.3) DMMB assay

The sulfated glycosaminoglycan (GAG) content of the samples was quantified by a dimethylmethylene blue (DMMB) dye assay (Sigma) [69]. Chondroitin sulfate

(CS) stock solution was prepared by dissolving 0.0875g cysteine in 50mL PBE and then adding 50mg CS into 1mL of PBE/cys solution. Working CS solution was prepared by dissolving 25μL of CS stock in 12.5mL of PBE/cys solution. Dimethlmethylene blue (DMMB) dye was prepared by adding 3.04g glycine, 2.37g NaCL, and 95mL of 0.1M HCl in 905mL of dH_2O. 16mg DMMB was then well mixed and dissolved in this solution on a magnetic stirrer. pH was adjusted to 3 using concentrated HCl. Absorbance of the DMMB solution was checked to ensure that OD_{525} was in the range of 0.31 and 0.34. For measurements, 20μL of papain-digested muscle samples and 80μL of dH_2O were combined with 2.5mL of DMMB reagent solution in 3mL disposable plastic cuvettes. Absorbance at 525nm was read using a Beckman Coulter spectrophotometer. Samples were extrapolated against CS standards between 0μL and 60μL of working CS solution (100μg CS/mL in PBE/cys solution).

2.2.2.4) Hydroxyproline assay

About 100 μL of papain-digested sample was combined with 900μL of 6M HCl and hydrolyzed on a heating block at 110-120°C for 18 hours in 2mL lockable microtubes. pH 6 buffer was prepared by dissolving 17g NaOH, 25g citric acid monohydrate, 60g sodium acetate trihydrate, and 60mL of glacial acetic acid in 250mL of dH_2O. The volume of the solution was brought up to 500mL by adding 244mL of dH_2O. Additional 150mL of isopropanol, 100mL of dH_2O, and 5 drops of toluene were added to the solution. Concentrated HCl was used to bring the pH to 6. Before measuring absorbance, acid-hydrolyzed samples were mixed with 2 drops of methyl red and neutralized with approximately 2mL of 2.5M NaOH, 2-3 drops of

0.5M HCl, and 1-2 drops of 0.5M NaOH. The volume of the neutralized hydrolyzates was brought to 3mL with dH_2O. About 1mL of the diluted samples was transferred to clean empty labeled 2mL microtubes before assaying. Samples were then combined with 0.5mL of freshly made Chloramine T, containing 0.705g Chloramine T (EMD) in 40mL of pH 6 buffer and 5mL of isopropanol, and incubated for 20 minutes at room temperature. Samples were subsequently mixed with 0.5mL of fresh pDAB, consisting of 7.5g *p*-Dimenthylaminobenzaldehyde (Sigma) in 30mL of isopropanol and 13mL of 60% perchloric acid, incubated in 60°C water bath for 30 minutes, and afterwards chilled on ice. Both Chloramine T and pDAB solution were made 24 hours prior to the experiment. Absorbance at 550nm was read on a Beckman Coulter spectrophotometer in 3mL disposable plastic cuvettes. Samples were extrapolated against hydroxyproline standards (trans-4-Hydroxy-L-proline: Aldrich) between 0μL and 700μL of working hydroxyproline solution (10μg/mL).

2.2.2.5) DNA assay

Total DNA content for papain-digested tissue samples was quantified as per the manufacturer's instructions using fluorescent Quanti-iT PicoGreen reagent (Invitrogen). In brief, 1X TE working solution was made by diluting the concentrated buffer (200mM Tris-HCl and 20mM EDTA with pH 7.5) 20-fold with DNase-free distilled water. The working solution of the Quanti-iT PicoGreen reagent was prepared by making a 200-fold dilution of the concentrated solution with 1X TE buffer and protected from light by covering it with aluminum foil. The working solution of dsDNA (500ng/mL) was prepared by diluting the 100μg/mL stock solution of dsDNA

with 1X TE buffer. For sample analysis, every 1μL of papain-digested samples was combined with 99μL of 1X TE. An equal volume of Quanti-iT PicoGreen working reagent was added to both DNA standards and samples. Fluorescence was measured using a Beckman Coulter DTX 880 Multimode Detector (excitation: 480nm; emission: 520nm) in a 96-well plate. Samples were extrapolated against a lambda DNA standard with concentrations ranging from 0ng/mL and 250ng/mL.

2.2.3) Histology and staining

2.2.3.1) Hematoxylin and eosin

All histological analysis was performed on tibialis anterior muscles for all ages from both WT and *mdx* mice. Samples were fixed in Bouin's solution (Sigma) and embedded in paraffin for sectioning on a microtome with thickness of 10μm after a series of dehydration processes. The hematoxylin and eosin (H&E) staining procedure began with deparaffinization and rehydration of the sections. The sample sections were first incubated in CitriSolv, a xylene substitute, for 3 times, 5 minutes each. They were subsequently treated in 100% ethanol 3 times for 3 minutes each, 95% ethanol 3 times for 3 minutes each, 70% ethanol 3 times for 3 minutes each, and briefly rinsed with dH_2O. The sections were then incubated with Gill2 Hematoxylin (StatLab Medical Products, McKinney, TX) for 5 minutes, washed with tap water, treated in Eosin-Y (Richard Allan Scientific) for 1 minute, and washed with tap water again for several times to remove excess staining. Lastly, the sections were dehydrated by a series of incubation in 70% ethanol for 30 seconds, 95% ethanol for 30 seconds, 100% ethanol for 30 seconds, and CitriSolv for 30-45 seconds and mounted with glycerol.

2.2.3.2) Picrosirius red

Picrosirius Red Stain Kit (Polysciences, Inc.) was used to evaluate and quantify collagen fibrils on paraffin-embedded samples. The sections were first deparaffinized and rehydrated in dH_2O. They were treated with Solution A for 2 minutes, washed with dH_2O, incubated in Solution B for one hour, placed in Solution C for 2 minutes, and then incubated in 70% ethanol for 45 seconds. The sections were then dehydrated and mounted with glycerol. Fibrosis for each age group was quantified based on 3 random images using ImageJ.

2.2.3.3) Safranin-O

Safranin O staining was performed on paraffin-embedded sections to visualize glycosaminoglycans (GAGs). Samples were first rehydrated in dH_2O and then incubated with 0.1% Safranin O solution (Sigma) for 15 minutes at room temperature. After washing with dH_2O, sections were dehydrated and mounted with glycerol.

2.2.4) Cross-sectional area (CSA) analysis

Cross-sectional area (CSA) of myofibers from the tibialis anterior muscles of all ages in both WT and *mdx* mice was determined using the Area function of the ImageJ Software on bundles in hematoxylin and eosin stained muscle sections at a magnification of 20X based on 3 to 5 random fields of view. Frequency plots were generated based on the CSA of muscle fibers. Distribution curves were fitted using GraphPad Prism 6.

2.2.5) SEM analysis

The morphology of TA muscles of WT and *mdx* mice was examine using scanning electron microscopy (SEM, Philips XL30 ESEM). In brief, samples were dehydrated in 50%, 75%, and 100% ethanol and then air-dried. The dried samples were then sputter-coated with Ir for 10 seconds (Emitech K575X Sputter Coater) prior to the SEM imaging.

2.2.6) Statistical analysis

All biochemical assays data were presented as mean ± standard deviation. For cross-sectional area (CSA) analysis, outliers were determined and removed from the data set, and the averaged distribution of CSA was analyzed across all ages of WT and *mdx* mice. Statistical significance was determined by either two-tailed unpaired Student's *t*-test or single-factor analysis of variance (ANOVA) with Tukey multiple comparison tests using GraphPad Prism 6 statistical software.

2.3) Results

2.3.1) Biochemical assays

Since there have been numerous reports on the age-associated and disease-related pathological fibrosis in skeletal muscle [65, 70, 71], we first evaluated the amount of collagen present in several different hindlimb muscles, including extensor digitorum longus (EDL), tibialis anterior (TA), and quadriceps (QUAD), of both WT and *mdx* mice with various ages. As shown in Fig. 5A, we observed significantly increased amount of collagen in EDL and TA muscles with aging in WT mice while QUAD muscles showed a slight increase in total collagen content with aging.

Similarly, dystrophic mice also showed the same trend as WT mice that the amount of collagen in EDL, TA, and QUAD muscles of mdx mice was significantly increased with aging (Fig. 5B). To further investigate the changes that skeletal muscle ECM undergoes with pathology-associated fibrosis, we compared the amount of collagen in EDL, TA, QUAD muscles between WT and their age matched *mdx* counter parts (Fig. 5C). Higher amount of collagens was observed in dystrophic mice within the same ages and the differences were much more distinctive in older mice (2mo).

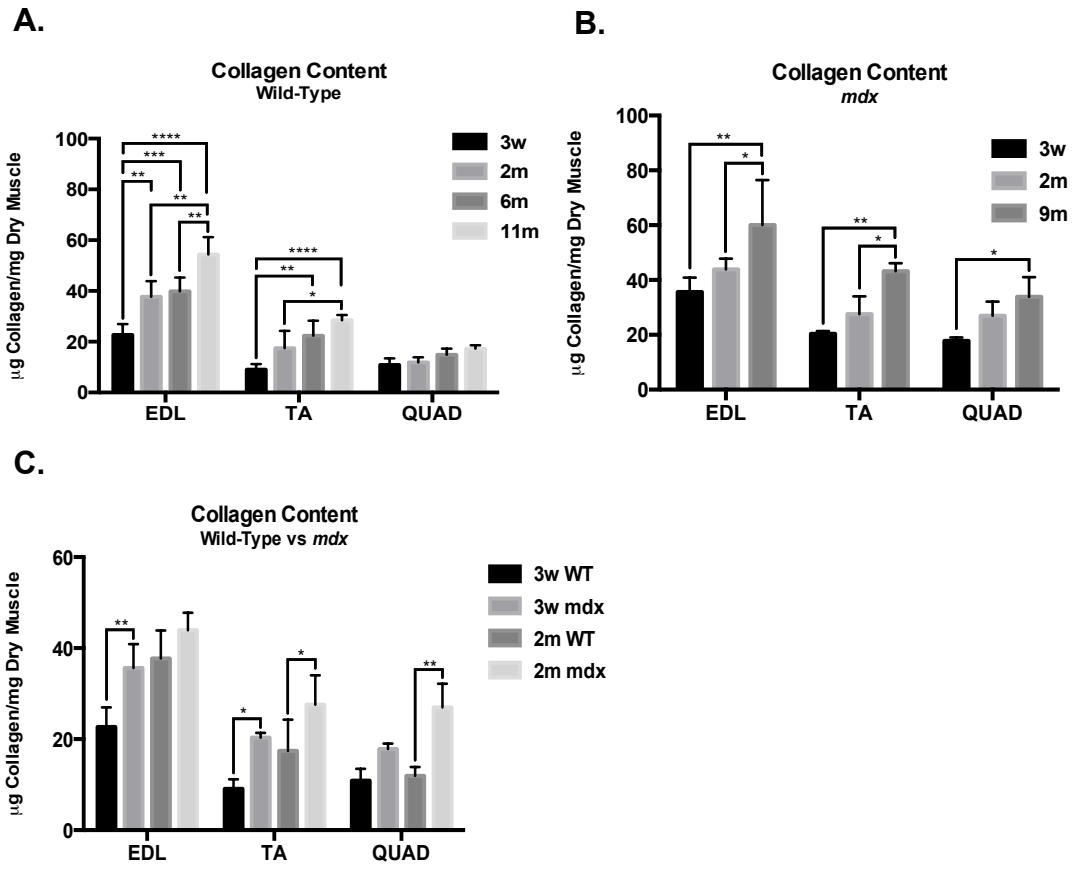

Figure 5. Total collagen content for WT and *mdx* male mice.
Collagen assay was done by performing the hydroxyproline assay. Comparison was made between different age groups for (A) WT mice, (B) *mdx* mice, and (C) both WT and *mdx* mice at 3w and 2m. Results are shown as the mean of biological replicates +/- standard deviation. ****p < 0.0001, ***p < 0.001, **p < 0.01, *p < 0.05.

Next, we investigated the changes of glycosaminoglycan (GAG) in EDL, TA, and QUAD muscles of WT and dystrophic mice as a function of age. As seen in Fig. 6A, we observed a significant decrease in the total amount of GAG in WT mice with aging. Similar trend was observed for *mdx* mice with aging and the changes in GAG contents were much significant as compared to the differences found in WT mice (Fig. 6B). To further evaluate the differences in the amount of GAG content between WT and *mdx* mice with varying ages, we compared the amount of GAG for EDL, TA, and QUAD muscles from WT with those from *mdx* mice at the age of 3wk and 2mo. As shown in Fig. 6C, we observed a higher amount of GAG in *mdx* mice as compared to the corresponding WT mice with matching ages. Such increase was clearly seen from all muscle types.

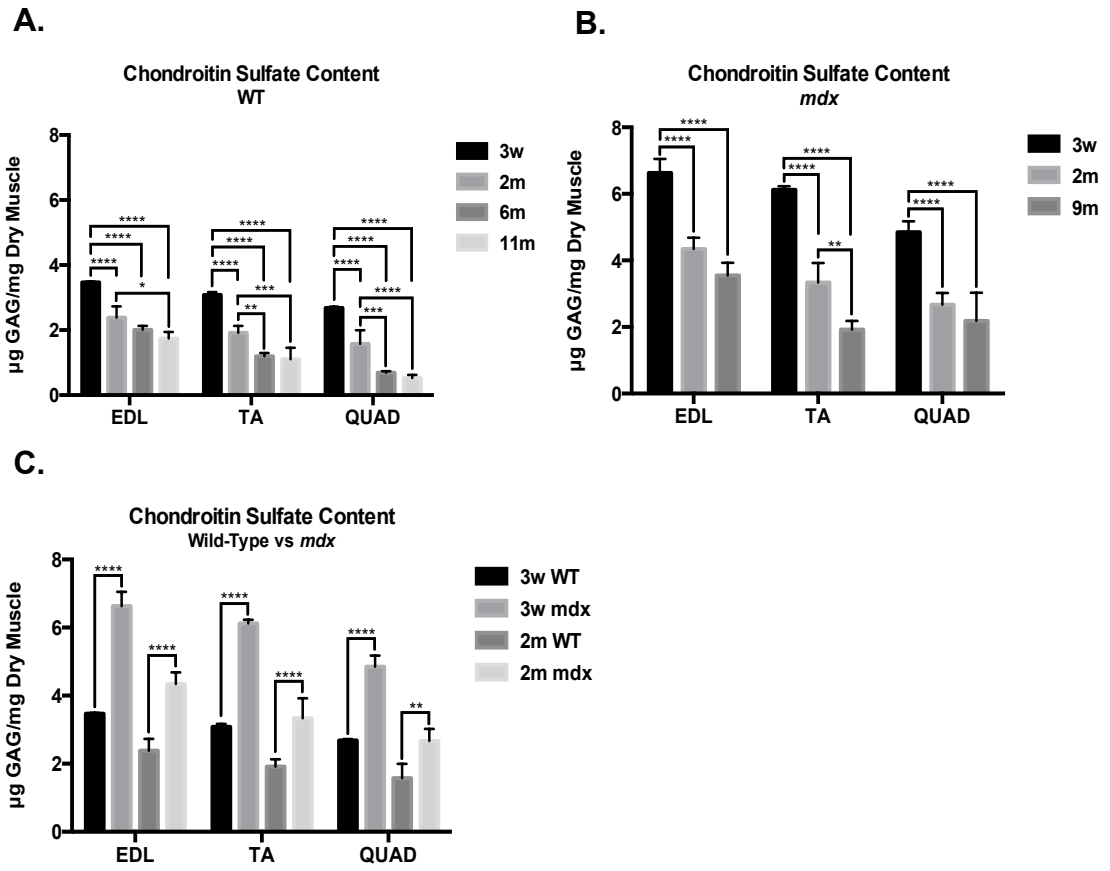

Figure 6. Total Sulfated GAG content for WT and *mdx* male mice.
GAG assay was done by performing the DMMB assay. Comparison was made between different age groups for **(A)** WT mice, **(B)** *mdx* mice, and **(C)** both WT and *mdx* mice at 3w and 2m. Results are presented as the mean of biological replicates +/- standard deviation. ****$p < 0.0001$, ***$p < 0.001$, **$p < 0.01$, *$p < 0.05$.

To evaluate the changes in cellular component of muscle, if any, as a function of age and muscle pathology, DNA content was examined for different age groups of WT and *mdx* mice. As shown in Figure 7A and 7B, there is an overall decrease in the amount of DNA content with an increase in age throughout all muscles types for both WT and *mdx* mice although the decrease seems to plateau from 6mo to 11mo for WT mice. As we compared DNA content for age-matched muscle samples with different muscle pathology, *mdx* mice, in general, tend to possess more cellular content than

WT mice, with an exception of 3wk EDL (Figure 7C). The difference, however, was only significant for 3wk TA and 2mo QUAD.

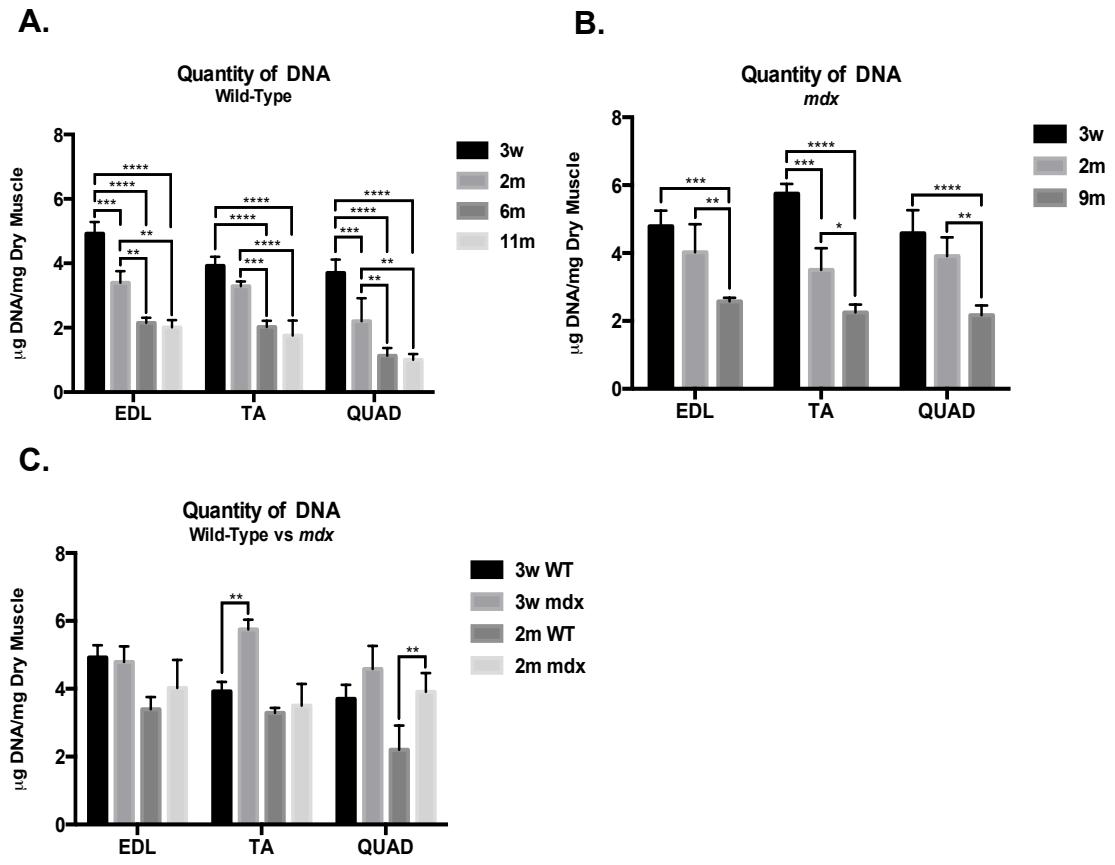

Figure 7. Total DNA content for WT and *mdx* male mice.
DNA assay was performed using the fluorescent Quant-iT PicoGreen reagent. Comparison was made between different age groups for (A) WT mice, (B) *mdx* mice, and (C) both WT and *mdx* mice at 3w and 2m. Results are presented as the mean of biological replicates +/- standard deviation. ****p < 0.0001, ***p < 0.001, **p < 0.01, *p < 0.05.

2.3.2) Histology

To corroborate the results from biochemical analysis, we also determined the histological changes in muscles of WT and *mdx* mice with varying ages. As shown in Fig. 8, H&E staining of various TA muscles revealed an increase in infiltration of fibrotic tissue with aging in both WT and *mdx* mice, and such fibrotic tissues present

within and near the myofibers were more significant in *mdx* than their corresponding age matched control (WT mice). Also, in *mdx* mice, we observed an increased number of myofibers having center-located nuclei with aging (Fig. 8B).

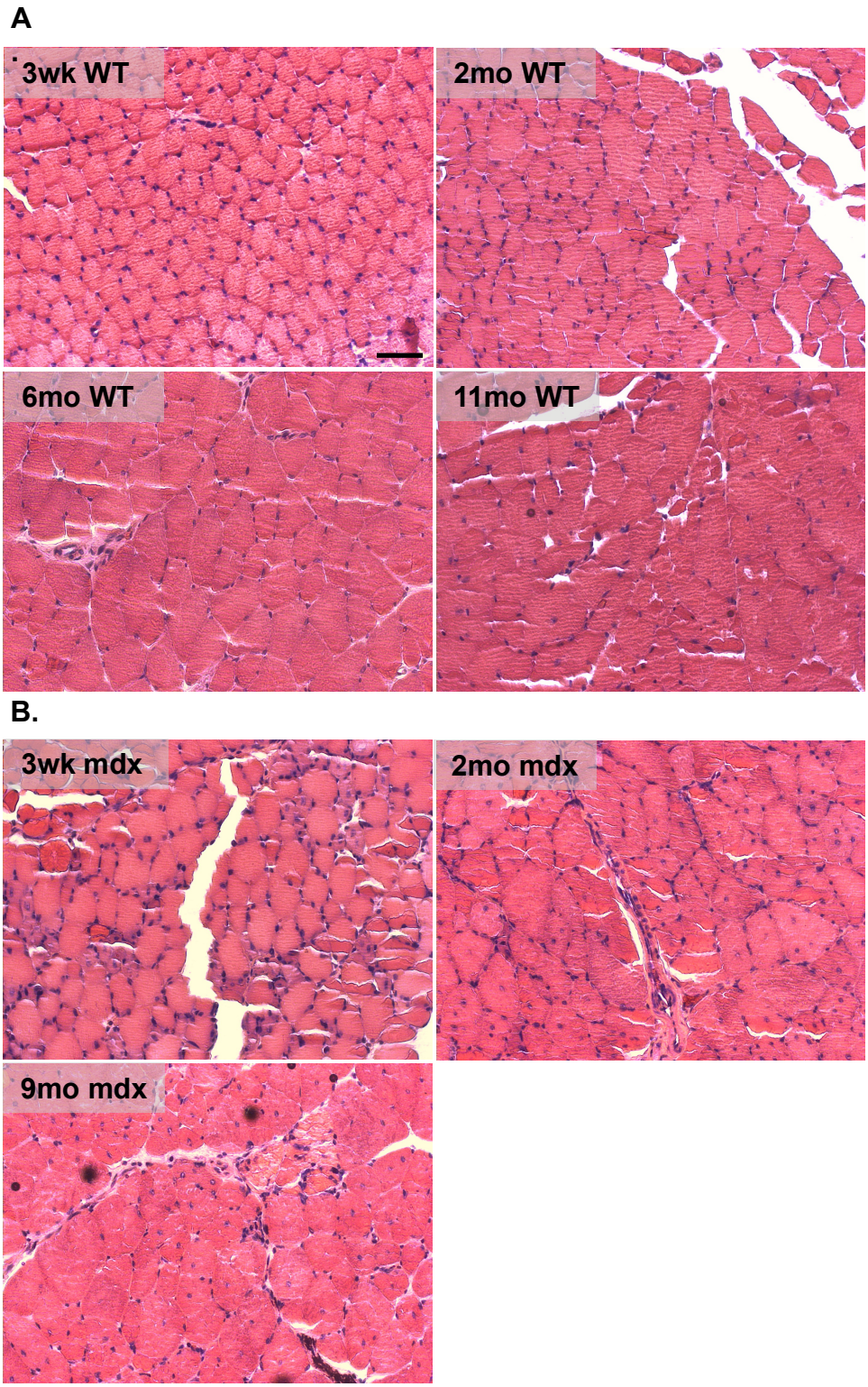

Figure 8. Hematoxylin and eosin staining analysis for myofiber structures.
Hematoxylin and eosin staining was performed on TA from different age groups of (A) WT and (B) *mdx*. Scale bar = 100μm.

To further validate the increased fibrosis in TA muscle, we performed Picrosirius Red staining, which demonstrates severe fibrosis in TA muscle with aging and *mdx* pathology (Fig. 9). As we observed, with an increase in age, there was a clear, correlated increase in collagen deposition throughout the muscle samples, and the differences became much obvious in the case of dystrophic mice. For quantitative analysis of fibrosis, we measured the positively stained area of Picrosirius Red, which visualizes the collagen deposition within the myofibers. Quantification of these fibrotic areas showed that fibrosis increases as a function of age and *mdx* pathology (Fig. 9B-C).

Next, to evaluate the changes in GAG contents within TA muscle, Safranin-O staining was performed on various TA muscles from WT and *mdx* mice with different ages (Fig. 10). However, due to the significant amount of GAG present in TA muscles irrespective to the ages and muscle pathology, we could not visually reveal the quantitative changes in GAG content within various TA muscles.

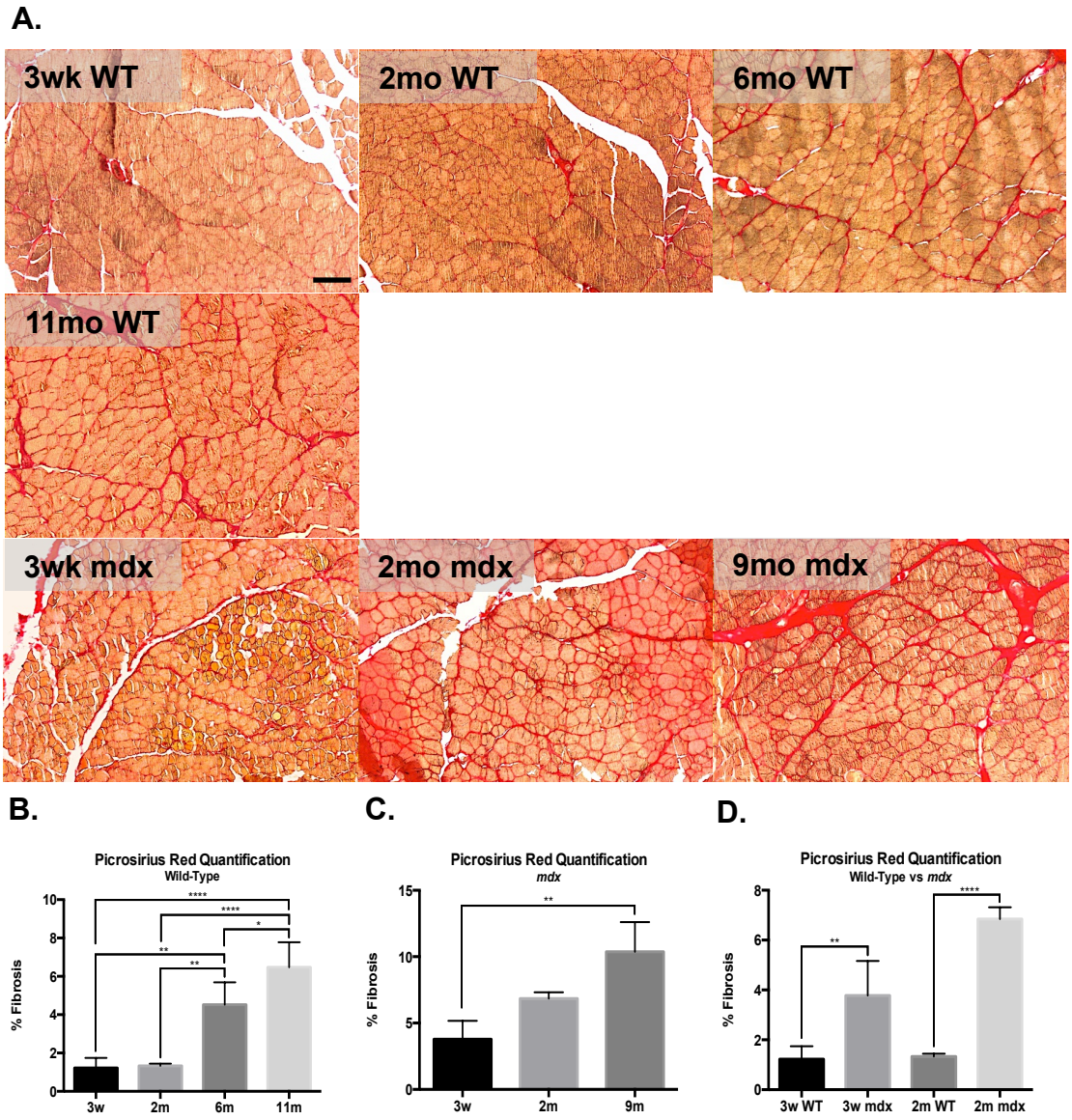

Figure 9. Picrosirius red staining analysis for percent of fibrosis.
(A) Picrosirius red staining was performed on TA for different WT and *mdx* age groups. Areas of fibrosis, which was stained red, were calculated for **(B)** WT, **(C)** *mdx*, and **(D)** WT vs *mdx*. Results are presented as the mean of biological replicates +/- standard deviation. ****p < 0.0001, ***p < 0.001, * *p < 0.01, *p < 0.05. Scale bar = 200μm.

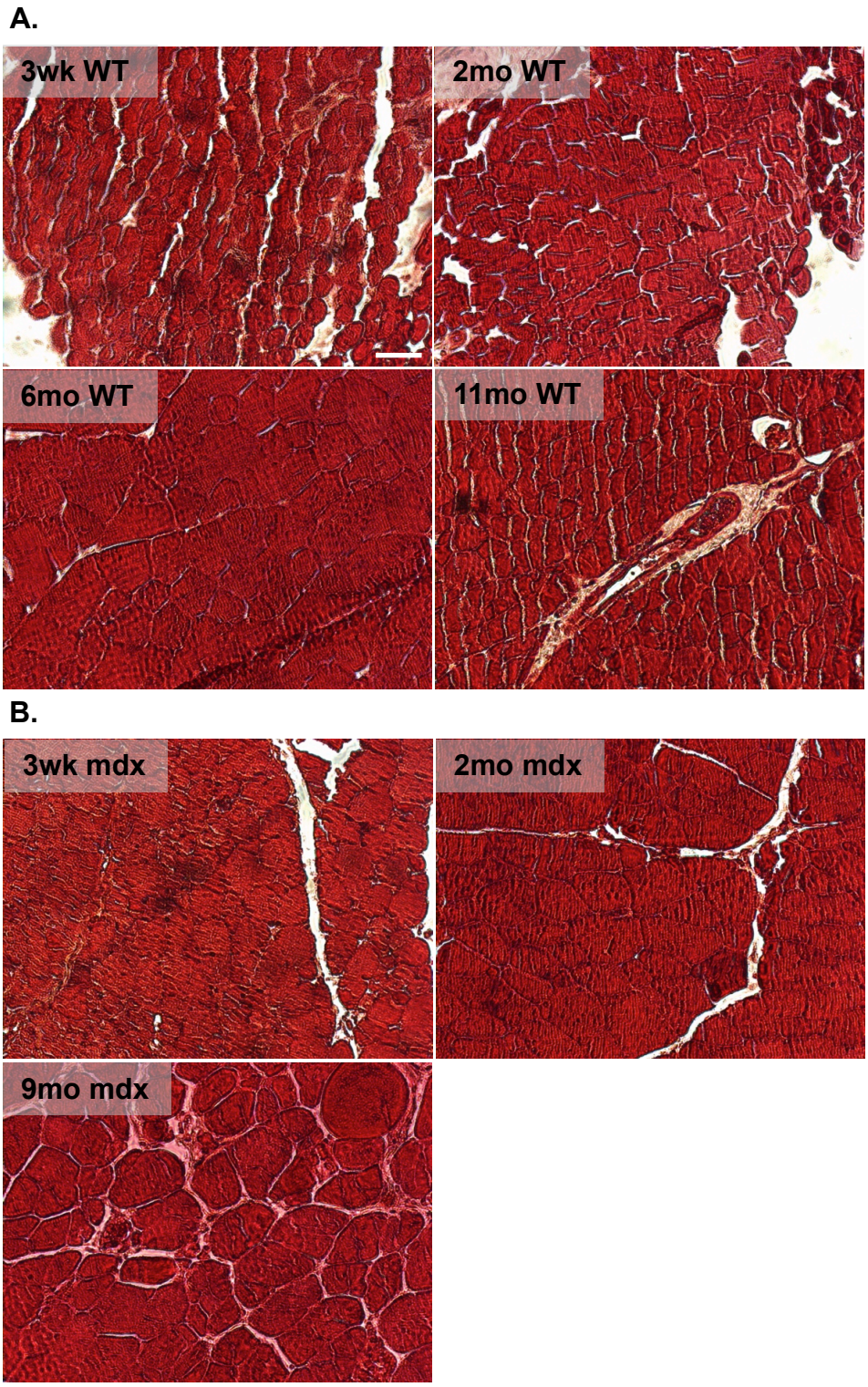

Figure 10. Safranin-O staining analysis for GAG content.
Safranin-O staining was performed on TA from different age groups of **(A)** WT and **(B)** *mdx*. Scale bar = 100μm.

2.3.3) CSA analysis

To further examine changes in muscle morphology in terms of aging and *mdx* pathology, we analyzed the CSA of myofibers based on 3 to 5 random fields of view from hematoxylin and eosin staining of WT and *mdx* TA muscles. As seen in Fig. 11, there is an overall significant increase in the averaged cross-sectional area of myofibers with age for both WT and *mdx* mice. The dramatic increase in the averaged size of myofibers for WT mice was observed from 3wk to 2mo, and thereafter the increase in the muscle bundle sizes seems to be flattened (Fig. 11A). For *mdx* mice, we observed the same trend that the majority of myofibers undergoes hypertrophy as age increases from 3wk to 9mo (Fig. 11B). When compared WT to *mdx* mice, we observed a higher averaged CSA in myofibers of *mdx* mice (Fig. 11C), indicating the presence of hypertrophied muscle bundles with *mdx* pathology. To more closely look at the differences in muscle bundle sizes in terms of aging and *mdx* pathology, we generated CSA distribution curves (Fig. 11D-F), and the curves revealed a shift towards larger fiber CSA with aging in WT mice (Fig. 11D). Also, such a shift was more evident in *mdx* mice, suggesting that there is a larger number of muscle fibers underwent hypertrophy in *mdx* mice (Fig. 11E). In addition to increased number of hypertrophied muscle fibers present in dystrophic mice, we also observed an increased number of atrophied myofibers in elder *mdx* mice. Lastly, when compared the CSA of WT myofibers with their counterparts at age of 3wk and 2mo, we observed an apparent shift in the distribution towards larger fiber sizes at both 3wk and 2mo (Fig. 11F).

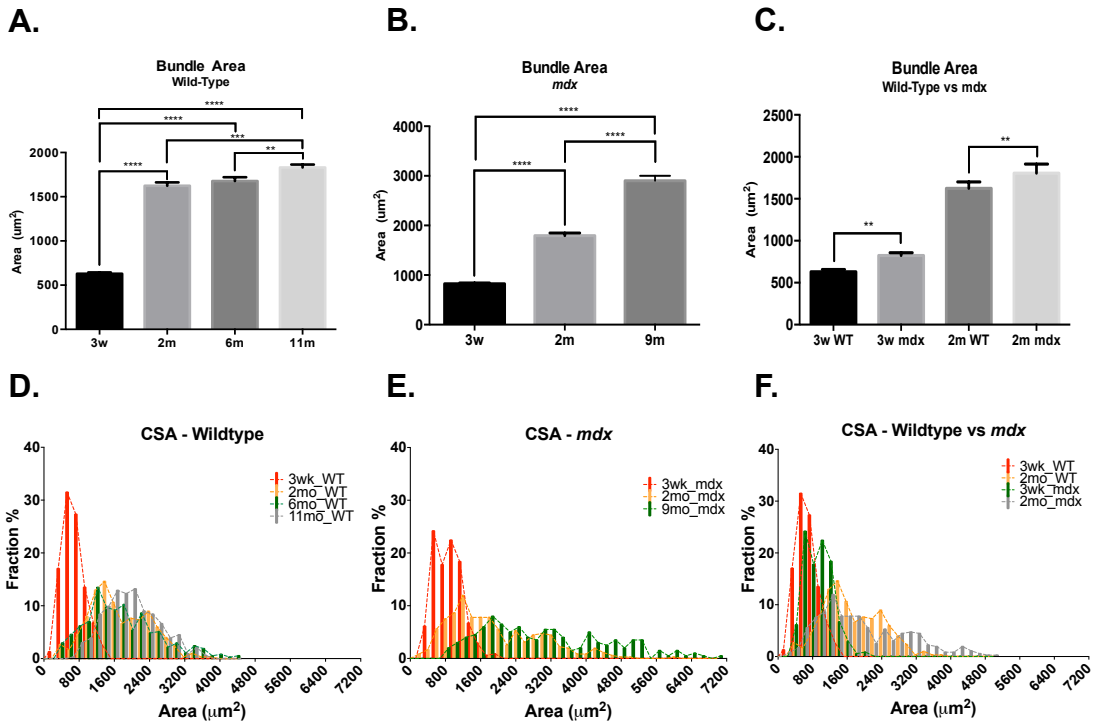

Figure 11. Myofiber cross-sectional area and fiber diameter analysis.
Averaged cross-sectional areas +/- standard error of the mean were calculated for **(A)** WT, **(B)** *mdx*, and **(C)** WT vs *mdx*. The frequency plots of cross-sectional areas were graphed for **(D)** WT, **(E)** *mdx*, and **(F)** WT vs *mdx*. ****p < 0.0001, ***p < 0.001, **p < 0.01, *p < 0.05.

2.3.4) Image analysis

To assess the age- and disease-associated microstructural and morphological changes of skeletal muscles, we performed SEM analysis on TA muscles from WT and *mdx* mice with varying ages. As shown in Fig. 12A, SEM analysis revealed an excessive deposition of fibrous ECM around the myofibers, and a close observation of the area between the myofibers suggests the presence of fibrous collagen. This phenomenon was shown as a function of age of the mice as it was more evident from 6mo and 11mo WT mice. Similar to the WT mice, *mdx* mice also have excessive fibrous ECM even in the younger mice, and this disease-related pathological fibrosis was much apparent in 9mo *mdx* mice (Fig. 12B). Thus, in accordance with previous

Picrosirius Red staining, the SEM analysis well corroborated the presence of excessive amount of fibrous collagen around the myofibers as a function of age and pathological condition of the mice.

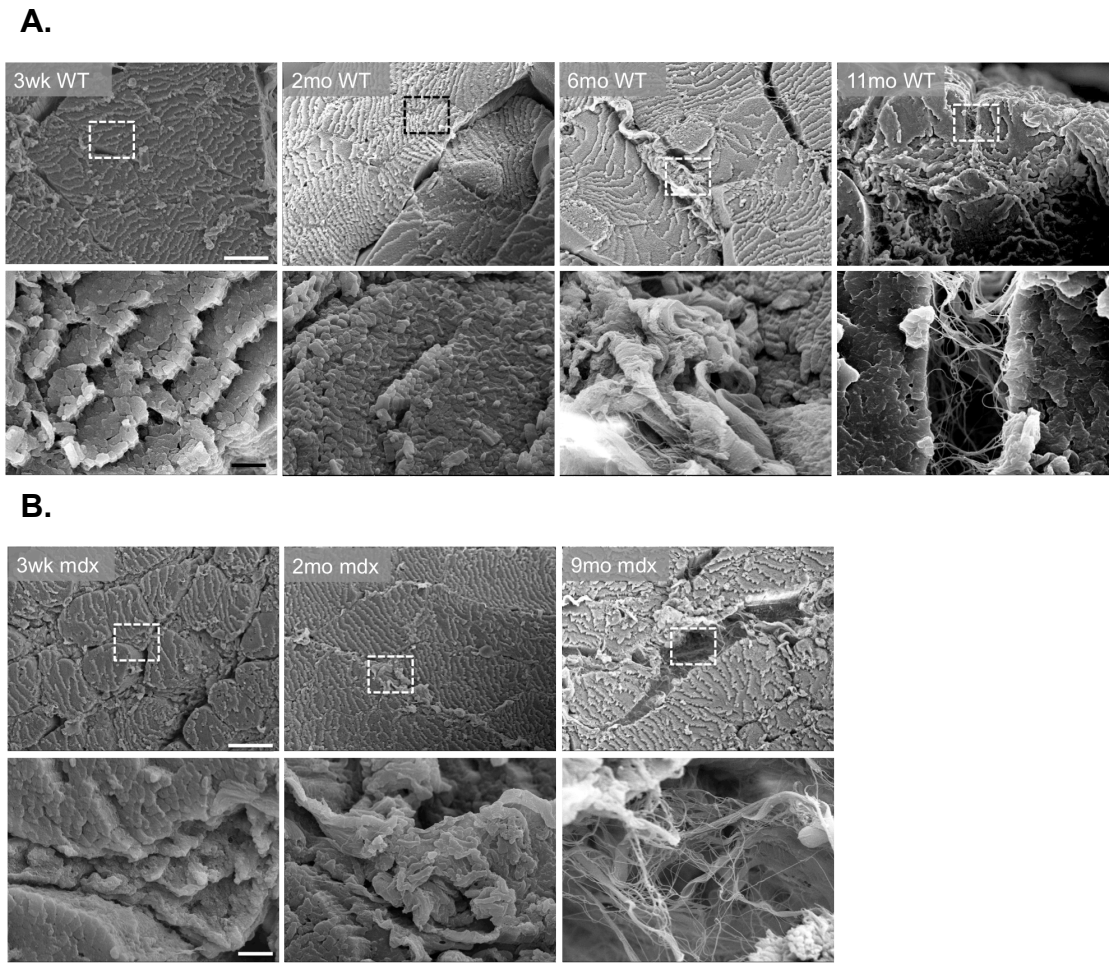

Figure 12. SEM analysis of WT and *mdx* muscles at different ages
Scanning electron micrographs were taken on TA from different ages of **(A)** WT and **(B)** *mdx*. Scale bar = 20, 2μm.

2.4) Discussion

Over the last decade, there has been a substantial number of studies documented the age- and disease-associated impairment in physiological function and regenerative potential of skeletal muscle. For instance, the ability to regenerate

skeletal muscle declines dramatically with aging while the amount of tissue fibrosis increases [54, 57, 63]. Furthermore, several studies have shown that muscle atrophy or wasting is inevitable in the process of aging [70]. However, how the biochemical cues in the ECM play a role in the progress of disease or aging still remains unclear. In this study, we aim to better understand the underlying biochemical and structural changes in the extracellular matrix of skeletal muscles in terms of aging and pathology by using normal healthy (WT) mice and muscular dystrophy (*mdx*) mice. Specially, we looked at the quantitative changes in collagen, glycosaminoglycan (GAG), and DNA content as well as some of the key morphological changes of muscle fibers associated with aging and muscle pathology.

Being the most abundant protein in the ECM, collagen contributes to the mechanical properties of the tissue, giving its tensile and elastic strength, and at the same time participates in the regulation of cell differentiation and attachment. It is well documented that the amount of collagen increases significantly with an increase in age, correlating with increased stiffness typically found in aged muscles [54, 72, 73]. Such an increase in collagen content might attribute to the increased cross-linking of collagen, resulting in resistance of fibers to collagenase degradation, as well as decreased enzymatic activity of these collagenases in older ages [54, 67]. As compared to previous studies, our study showed a similar result of an increased content with aging, but the difference of collagen concentration was not significantly found in QUAD, suggesting that there is variation in the ECM composition of different muscle types. Dystrophic pathology, on the other hand, is well known for its

characteristic of excessive collagen composition. Numerous studies have demonstrated that dystrophic mice express an excessive fibrosis as characterized by accumulation of collagen due to chronic inflammation and persistent activation of myofibroblasts [54, 67, 68, 74, 75]. In addition, an accumulation of collagen has been found to associate with increased transcriptional activity of collagen in response to muscle fiber damage in *mdx* mice [67]. Thus, it is not surprising to find a significantly higher quantity of collagen and a greater percentage of fibrosis in *mdx* mice than in WT mice at the same ages.

Glycosaminoglycan (GAG) is found to be a long sulfated carbohydrate chain covalently attached to a core protein, forming an abundant macromolecule in ECM called proteoglycan. Previously, proteoglycans have been known to play an important role in regulating various cellular processes, such as proliferation, differentiation, and regeneration of various tissues [76-78]. In skeletal muscle, proteoglycans have been shown to modulate myogenic differentiation through cellular activities like cell differentiation [79, 80]. When the skeletal muscle become aged, there is a significant decrease in the total GAG content in both wild-type and *mdx* mice [53]. When we compared the amount of GAG between age-matched WT and *mdx* mice, we observed that *mdx* mice, in general, tended to have higher GAG content than WT. Since some types of proteoglycans, such as decorin and biglycan, were reported to be actively participated in the regeneration process by serving as a link between muscle fibers and ECM to compensate the absence of dystrophin in *mdx* mice as well as mediating cellular signaling among various growth factors, it is not surprising to find the

accumulation of GAG in *mdx* mice as these diseased mice constantly undergo regeneration to compensate the muscle fiber degeneration [55, 81]. Previously, Caceres et al. have successfully demonstrated that the amount of proteoglycans in dystrophic mice was significantly increased during the skeletal muscle regeneration [82].

Another aspect of aging appears to be a decreased number of muscle fibers and other cellular components in ECM as well as changes in the overall muscle mass. As previously reported, aging has been associated with various degree of atrophy or hypertrophy of muscles [83]. For example, several studies have demonstrated that with aging, there was significant loss of muscle mass due to a decline in the number of muscle fibers as well as the size of muscle cells [84-86]. Moreover, Lexell *et al* has found that the reduction in muscle mass can occur as early as 25 years of age in human and it typically accelerates after the age of 50, and such reduction is more a result of decreased fiber number than reduced fiber size [87, 88]. One recent study showed that the fiber loss with aging may vary among different muscle types and locations of the muscles using mouse skeletal muscles [89]. In the present work, we evaluated the age- and disease-associated changes in fiber size and cell number through cross-sectional area analysis and DNA quantification.

The results of DNA quantification demonstrated that there was an overall decrease in the total population of cellular components with aging in both WT and *mdx* mice. Previous studies have demonstrated that regenerative capacity of skeletal muscle diminishes with aging due to the change in resident stem cells, satellite cells,

and diminished activation of these cells [57, 90]. In addition, Barazzoni *et al* have shown substantial mitochondrial DNA depletions with aging due to oxidative damage occurring in aged muscles [91]. Our observation of the decline in total DNA content with aging could be a result from depletions in mitochondrial DNA as well as the decreased number of myofibers. In the case of dystrophic mice, we observed an overall trend of *mdx* mice having more DNA content than WT mice at the same age, especially in TA and QUAD. Such trend was further validated in TA muscle through hematoxylin and eosin staining in which an increased amount of nuclei was stained in *mdx* mice. Kottlors' group has found an elevated satellite cell number in those with muscular dystrophy [92]. In addition, Porter *et al* showed that dystrophin-deficient mice are continuously in the state of fiber degeneration associated with chronic inflammation [66]. All these pathologies together could possibly contribute to the increase in the number of cells in the local ECM and up-regulated cellular activities. However, further studies are necessary to target specific cell populations associated with aging and fibrotic pathology.

The estimated averaged cross-sectional area (CSA), on the other hand, seemed to increase slowly after 2mo in the case of WT mice. As skeletal muscles undergo development, the muscle mass increases as individual fibers grow in size. When the growth stage is passed, muscle fibers typically experience atrophy or shrinkage in size with aging [93]. In *mdx* mice, the continuous increase in the size of muscle fibers indicates the phenomenon of hypertrophy generally found in muscle fibers of dystrophic mice [71]. To further evaluate the morphological changes in muscle fibers

with aging and disease, we generated the distribution curve and observed an overall shift towards larger fiber size in both WT and *mdx* mice. In addition, the fitted curves showed a more heterogeneous distribution of fiber sizes in *mdx* mice as compared to the distribution of the age-matched WT mice. Such heterogeneity in fiber sizes suggests that the dystrophic mice possess both atrophied and hypertrophied myofibers associated with the perpetual degeneration and regeneration these diseased mice normally experience [30, 71].

2.5) Conclusion

This study demonstrates the distinctive quantitative changes in the extracellular matrix composition and structure in terms of aging, muscle types, and muscle pathology. In particular, our results show an increase in collagen content and a decrease in sulfated glycosaminoglycan and DNA content with aging. Comparing between WT and *mdx*, *mdx* mice possess significantly more collagen and glycosaminoglycan than WT mice at the same age, but there is only a slight increase in the amount of DNA in *mdx* mice than in WT mice. In addition, an increase in cross-sectional area of muscle fibers, fiber diameter and fibrosis is observed with aging and between WT and *mdx* mice. In conclusion, aging and muscle pathology are crucial factors that can affect the extracellular matrix of skeletal muscles.

2.6) Acknowledgement

Chapter 2, in full, is currently being prepared for submission for publication of the material: Xie, Yun; Chauhan, Ruvi; Hwang, Yongsung; Lin, Susan; Seo, Timothy;

Varghese, Shyni. The thesis author was the primary investigator and author of this paper.

CHAPTER 3: THE ROLE OF ECM ON FIBROSIS PROGRESS IN SKIN

3.1) Introduction

Skin, being the largest organ in human body, is a complex, multilayer organ that serves as a barrier to prevent invasion of foreign substances and disturbance from environmental stresses. Skin consists of two major layers, epidermis and dermis, separated by basal membrane [94]. Epidermis, as the outermost layer, protects the body from water loss and at the same time maintains body temperature. Epidermis consists of four major layers: stratum corneum, granular cell layer, spinous layer, and basal layer. Stratum corneum is a thick outer layer of flattened keratinized non-nucleated cells, which typically help protect body from trauma and infection. Granular cell layer primarily serves as a water barrier whereas spinous layer is considered a layer of differentiated stem cells. Basal layer, which is closest to dermis, is a natural reservoir for epidermal stem cells [95]. Dermis, on the other hand, is considered as the connective tissue layer, providing tissue with tensile and elastic strength. Dermis predominantly consists of collagen, elastic fibers, and a small fraction of other extracellular matrix components. Most importantly, dermis is the main residing place for resident fibroblasts, which contribute to skin fibrosis once they transition into abnormal state [94].

Skin fibrosis, also referred as scleroderma, is a chronic disorder associated with excessive deposition of extracellular matrix, mainly type I collagen, in the dermis. As the disease progresses, not only the skin is affected, but also other internal organs may become dysfunctional, leading to life-threatening consequences [24]. Currently,

there are no effective treatments for fibrosis in skin. Thus, it is crucial to understand the underlying mechanisms of this disease.

Previously, one of our collaborators, Dr. Colin Jamora, has established a fibrotic skin model from transgenic mice, which exogenously express a transcription factor Snail in the epidermis of the skin, leading to severe inflammation and fibrosis in the dermis, similar in the case of tumor formation [96]. Snail is a transcription factor that has been known for its role in embryogenesis for facilitating tissue formation in a process called epithelial-mesenchymal transition (EMT) [97]. Not only in development, Snail also has been shown to induce renal fibrosis upon activation [98]. Jamora *et al* has demonstrated that the expression of Snail during hair follicle morphogenesis leads to proliferation of keratinocytes in the epidermis, which in turns invades the dermal compartment [99]. In addition to fibrotic pathology, Snail transgenic mice also have higher amount of collagen and elastin, resulting in a higher elastic modulus and thus increased stiffness in skin.

Emerging findings by Nakasaki et al., (from our group) have identified a specific molecule in the ECM that contributes to the fibrosis progression of skin. When Snail transgenic mice (fibrotic mice) were crossed with mice depleted of this particular molecule (Molecule X), the resulting Snail Tg/Molecule X knock-out mice (treated fibrotic mice) showed down-regulation in several representative gene markers of fibroblast activation. Furthermore, the treated fibrotic mice demonstrated a decreased amount of elastin and thus a decreased elastic modulus as compared to

fibrotic mice. All these findings suggest that the role of ECM properties can have an effect on the progression of skin fibrosis.

In this part of the thesis, we are interested in investigating how the ECM properties of skin may contribute skin fibrosis. Specifically, we employed decellularized skin tissues to mimic the biological environment and study how ECM alone can influence the activation of fibroblast in fibrosis progression of skin.

3.2) Materials and Methods

3.2.1) Animal handling

All animal procedures were in accordance with the guidelines of IACUC. Control wild type (WT) mice were raised in the lab's vivarium. Mice engineered to express the Snail transgene in the epidermis, which we called fibrotic mice here, were obtained as previously described [100]. The treated fibrotic mice were bred by crossing fibrotic mice and mice with depletion of a molecule which has been shown to play a role in skin fibrosis. To genotype the newly born mice, genomic DNA was extracted from the tips of the toes and analyzed with conventional PCR by using specific primers for each genotype. All mice were raised to Day 9 and processed for isolation of back skin.

3.2.2) Decellularization of skin tissues

Skin tissues were isolated from the back of the postnatal-day-9 (P9) mice that were either wild type, or fibrotic, or treated fibrotic and cut into 1 cm by 1 cm square. Samples were then either stored in -80°C or processed directly.

All decellularizing procedures and washing were carried out in the hood with sterile solutions. The prepared skin samples were first immersed in the 1M NaCl for 2 hours on a slowly moving four-way shaker under room temperature. The samples were then rinsed with Milli-Q H_2O and incubated in the fresh Milli-Q H_2O for 2 hours on the same slowly moving four-way shaker under room temperature. The 2hr-NaCl-2hr-H_2O cycles was repeated for 4 times under same conditions. The samples were then incubated in the freshly made DNase/RNase solution for 6 hours on a shaker under 37°C. The DNase/RNase solution was prepared by dissolving DNase I stock solution with concentration of 2.5mg/mL and RNase stock solution with concentration of 2mg/mL in the 50mM Tris-HCl buffer with 10mM $MgCl_2$. The final solution should have the DNase I concentration of 20μg/mL and the RNase concentration of 60μg/mL. After 6-hour incubation in nuclease solution, tissue samples were washed in fresh Milli-Q H_2O for overnight before incubating in sterilized PBS with 2% Penicillin Streptomycin (PenStrep) for 3-4 hours. Epidermis of the skin was peeled off as shown in Fig. 13 before treating with PBS consisted of 2% PenStrep. Fully decellularized tissues with epidermis removed were either processed directly or stored in -80°C for future use.

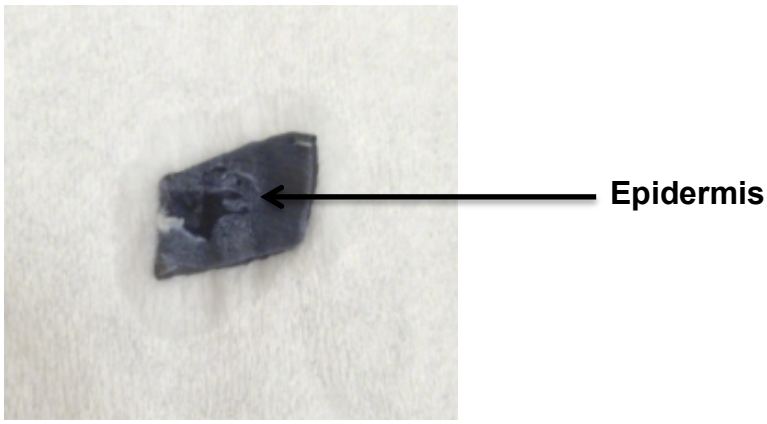

Figure 13. A photograph of decellularized skin before peeling of epidermis.
Isolated skin was decellularized based on the method described. After 2-day process, epidermis was peeled off to expose dermis of the skin before storage.

3.2.3) Biochemical assays

3.2.3.1) Tissue sample preparation

Both non-decellularized and decellularized skin samples were first processed into 5mm punch biopsies and then placed in labeled, pre-weighed empty 1.5mL Eppendorf tubes and snap-frozen in liquid nitrogen. Samples used in hydroxyproline assay and elastin assay were directly stored at -80°C while other tissue samples were either stored at -80°C for future use or lyophilized for 1-2 days directly. All dried samples were weighed to obtain dry weights.

3.2.3.2) Papain digestion

Dried skin tissues were digested with papain solution containing sterile papain and L-cysteine dissolved in PBE buffer. PBE buffer, with pH 6.5, was prepared by dissolving 7.1g Na_2HPO_4 and 1.86g Na_2EDTA in 500mL dH_2O. The buffer was then filter-sterilized and stored at 4°C for future use. To make papainase, 24.2g L-cysteine with formula weight of 121.16g/mol was first dissolved in 20mL of pre-made PBE buffer and then filter-sterilized. 0.10mL of sterile papain stock was added to this

solution through TB syringe and needle. Skin samples were grinded into pieces with pellet pestle after 1mL of prepared papainase was added to each sample. Fully homogenized samples were placed in water bath at 60°C for at least 16 hours.

3.2.3.3) DMMB assay

For DMMB assay, 20μL of papain-digested skin samples were first mixed with 80μL of dH_2O and then combined with 2.5mL of DMMB reagent solution in 3mL disposable plastic cuvettes. Absorbance was read using a Beckman Coulter spectrophotometer at 525nm. Samples were extrapolated against CS standards between 0μL and 60μL of working chondroitin sulfate (CS) solution (100μg CS/mL in PBE/cys solution). Working CS solution was prepared by dissolving 25μL of CS stock (0.0875g cysteine in 50mL PBE and then adding 50mg CS into 1mL of PBE/cys solution) in 12.5mL of PBE/cys solution prepared by dissolving. Dimethlmethylene blue (DMMB) dye was prepared by adding 3.04g glycine, 2.37g NaCL, and 95mL of 0.1M HCl in 905mL of dH_2O. 16mg DMMB was then well mixed and dissolved in this solution on a magnetic stirrer. The final solution had a pH of 3 and OD_{525} in the range of 0.31 and 0.34.

3.2.3.4) Hydroxyproline assay

About 200μL of 6M HCl was added to each 5mm skin biopsy punch and hydrolyzed on heating block at 95°C for 16 hours in 2mL lockable microtubes after vortexing vigorously. Then, about 10μL of hydrolyzed samples were aliquot into new tubes and placed on the 95°C heating block for evaporation of all liquids. The residues were then diluted with 200μL deionized H_2O. Before assaying, neutralized

hydrolyzates were combined with 0.1mL of freshly made Chloramine T, containing 0.705g Chloramine T (EMD) in 40mL of pH 6 buffer and 5mL of isopropanol, and incubated for 20 minutes at room temperature. Samples were subsequently mixed with 0.1mL of fresh pDAB, consisting of 7.5g *p*-Dimenthylaminobenzaldehyde (Sigma) in 30mL of isopropanol and 13mL of 60% perchloric acid, incubated in 60°C water bath for 30 minutes, and afterwards chilled on ice. Both Chloramine T and pDAB solution were made 24 hours prior to the experiment. pH 6 buffer was prepared by dissolving 17g NaOH, 25g citric acid monohydrate, 60g sodium acetate trihydrate, and 60mL of glacial acetic acid into 250mL of dH_2O. The volume of solution was brought up to 500mL by adding 244mL of dH_2O. Additional 150mL of isopropanol, 100mL of dH_2O, and 5 drops of toluene were added to the solution with final pH of 6. The prepared samples along with standards were transferred to a 96-well plate for measurement. Absorbance was read on a Bio-Tek Synergy HT1 microplate reader at 562nm. Samples were extrapolated against hydroxyproline standards (trans-4-Hydroxy-L-proline: Aldrich) between 0μL and 700μL of working hydroxyproline solution (10μg/mL).

3.2.3.5) DNA assay

Total DNA content for papain-digested tissue samples was quantified as per the manufacturer's instructions using fluorescent Quanti-iT PicoGreen reagent (Invitrogen). 1X TE working solution was made by diluting the concentrated buffer (200mM Tris-HCl and 20mM EDTA with pH 7.5) 20-fold with DNase-free distilled water. The working solution of the Quanti-iT PicoGreen reagent was prepared by

making a 200-fold dilution of the concentrated solution in 1X TE buffer and protected from light by covering it with aluminum foil. The working solution of dsDNA (500ng/mL) was prepared by diluting the 100μg/mL stock solution of dsDNA in 1X TE buffer. For sample analysis, every 1μL of papain-digested samples was combined with 99μL of 1X TE. An equal volume of Quanti-iT PicoGreen working reagent was added to both DNA standards and samples. Fluorescence was measured using a Beckman Coulter DTX 880 Multimode Detector (excitation: 480nm; emission: 520nm) in a 96-well plate. Samples were extrapolated against a lambda DNA standard with concentrations ranging from 0ng/mL and 250ng/mL.

3.2.3.6) Elastin assay

Total elastin content for 5mm biopsy bunched samples was quantified based on the manufacturer's instructions using Fastin Elastin Assay (Biocolor). Tissues were first placed in clean 1.5mL microcentrifuge tubes and heated at 100°C for two one-hour periods with 0.25M oxalic acid. Only 100μL of the combined supernatant from two incubations was transferred to new 1.5mL microcentrifuge tubes. Elastin standards were prepared by diluting 1.0mg/mL stock solution of elastin with dH_2O. An equal volume of Elastin Precipitating Reagent was then added to both standards and samples and incubated at room temperature for 15 minutes. After draining the liquids, 400μL Dye Reagent was mixed with the remaining pellets and rotated for 90 minutes. 250μL Dye Dissociation Reagent was then added to each sample. Absorbance at 513nm was measured using a Beckman Coulter DTX 880 Multimode

Detector in a 96-well plate. Samples were extrapolated against elastin standards between 0μg and 50μg of elastin.

3.2.4) Hematoxylin and eosin staining

Tissues frozen in Optimal Cutting Temperature (OCT; Sakura, Tissue-Tek) solution were first cryo-sectioned into 10μm sections parallel to hair shafts. The hematoxylin and eosin (H&E) staining procedure began with fixation in 4% paraformaldehyde for 10 minutes. The sample sections were subsequently washed with PBS for three times, 5 minutes each. Then, they were incubated with Gill2 Hematoxylin solution (StatLab Medical Products, McKinney, TX) for 5 minutes, washed with tap water, treated in Eosin-Y (Richard Allan Scientific) for 1 minute, and washed with tap water again for several times. Lastly, the sections were dehydrated by a series of incubation in 70% ethanol for 30 seconds, 95% ethanol for 30 seconds, 100% ethanol for 30 seconds, and CitriSolv for 30-45 seconds and mounted with glycerol.

3.2.5) Primary dermal fibroblast isolation

Primary mouse dermal fibroblasts were isolated from the back skin of postnatal day 3 (P3) C57BL/6 wild type mice. The P3 pups were first rinsed with 70% EtOH and sterile PBS in a 10cm petri dish before removing head, limbs, and tail. Both the back and belly skin was cut out and incubated in dispase with concentration of 250U/mL at 37°C for 1 hour. Epidermis was then separated from the dermis with a fine forceps. The isolated dermis was dipped in PBS and excess liquid was removed with paper towel. Next, the cleaned dermis was incubated in a 3mL solution

containing collagenase IV (2.5mg/mL in PBS) and 2 times gentamicin for 1 to 2 hours at 37°C with occasional agitation. The dermis was then incubated in a collagenase solution that was neutralized to a final concentration of 1mM by adding EDTA at room temperature for 5 minutes. The final volume was brought to 10mL with DMEM (Dulbecco's Modified Eagle Medium, Invitrogen), and the tube containing the final solution was vortexed vigorously for several times to ensure complete detachment of fibroblasts from collagen fibers. The fibroblast suspension was run through cell strainer to remove remaining debris. After centrifuging at 1000rpm for 5 minutes, aspirating the supernatant, and resuspending the cell pellets in 3mL complete media containing antibiotics, we then stored the isolated dermal fibroblasts in liquid nitrogen as frozen stock.

3.2.6) Primary dermal fibroblast culture

Frozen stock of dermal fibroblasts was thawed freshly for each experiment. Cells were maintained in DMEM (Invitrogen) containing 10% FBS (Fetal bovine serum, Thermo Fisher) and penicillin/streptomycin in a humidified incubator at 37°C with 5%CO_2. Cells were collected at the passage three to four after five days of culture. Before seeding the dermal fibroblasts on the decellularized skin, cells were resuspended to obtain a density of $2x10^5$ cells/mL. Each decellularized skin was first incubated in DMEM for two times, 15 minutes each, before placed in a well of 24-well plate (Corning) with agarose covering the plastic area. Prepared cell suspension was then added directly into the well containing the decellularized skin. A simple schematic that demonstrates culturing the fibroblasts on the decellularized skin was

shown in Fig. 14. Cells were cultured in the well for either 3 days or 7 days before extraction of RNA.

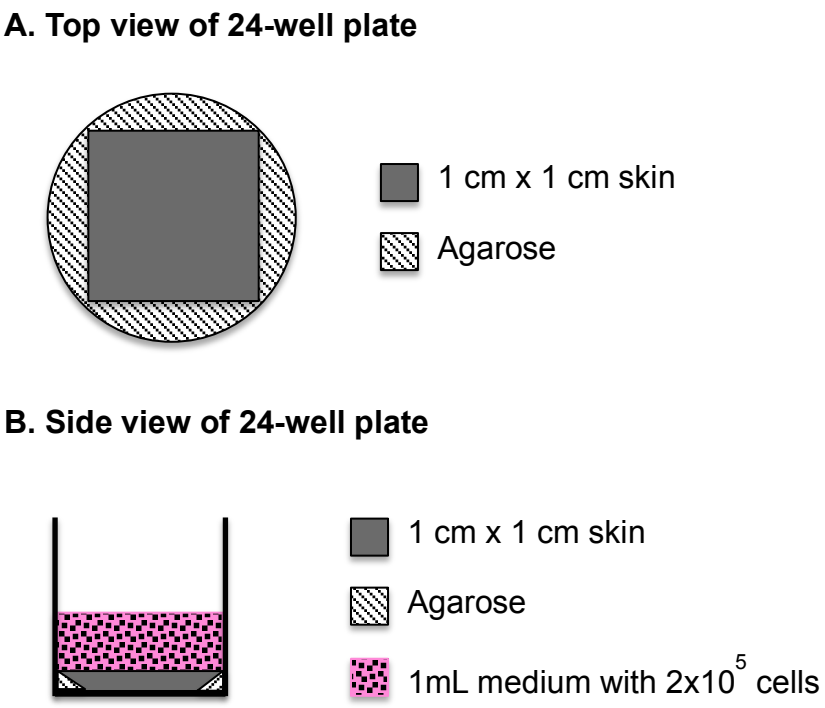

Figure 14. Simple schematic of primary dermal fibroblasts culture set-up.
1cm by 1cm decellularized skin was placed in the 24-well plate with agarose covering the plastic area to prevent cell adhering onto the plate. $2x10^5$ cells were suspended in 1mL of medium and plated directly on the skin. Here, both the top view **(A)** and side view **(B)** of one well in the 24-well plate were shown.

3.2.7) Extraction of RNA

Skin tissues with dermal fibroblasts cultured for either 3 days or 5 days were used for total RNA extraction based on a Trizol/RNeasy RNA extraction method. First, samples with complete removal of agarose were immersed in 1mL of Trizol (Invitrogen) for 10 to 15 minutes at room temperature. Supernatant was transferred to a new RNA-free 1.5mL tube, and about 0.2mL chloroform was then added to every 1mL of Trizol solution and incubated for 2 to 3 minutes under room temperature. After spinning down at 12000rcf for 15 minutes at 4°C, the top aqueous phase was

extracted and transferred to a new sterile RNase-free tube. The transferred solution was then run through the Qiagen's RNesay kit to purify the extracted RNA per manufacturer's instructions. Briefly, an equal amount of 100% RNA-free EtOH was first added to the lysate. Up to 700μL of the sample was transferred to the RNeasy Mini spin column and centrifuged for 15 seconds at 8000rcf. The remaining flow-through was discarded. Then, 700μL RW1 and 500μL RPE were added subsequently according to the previous step. Then, another 500μL RPE was added and centrifuged for 2 minutes at the same speed to discard the flow-through. Lastly, the RNeasy spin column was placed in a new 1.5 tube, and about 30-50μL of RNase-free water was added directly to the spin column membrane and centrifuged for 1 minute at 8000rcf to collect the final product.

3.2.8) Quantitative real-time PCR

Reverse transcription was performed on 1μg of total extracted RNA using the iScript cDNA Syntehsis Kit (BioRad). The resulting cDNA was used in real-time PCR per manufacturer's instructions with recommended SsoFast^{TM} EvaGreen® Supermix (Bio-Rad) on the CFX Real Time System c1000 Thermal Cycler real-time qPCR instrument (Bio-Rad). The relative fold expression was calculated from the Ct values based on the previously described method [101]. Sample sizes were n = 3 for wild type, Snail transgenic, and Snail transgenic/Fibulin-5 KO. The primer pair sequences are shown below as gene marker, forward primer sequence, and reverse primer sequence:

1. β-Actin: GGGCTATGCTCTCCCTCAC, GATGTCACGCACGATTTCC

2. αSMA: ATCGTCCACCGCAAATGC, AAGGAACTGGAGGCGCTG
3. SPARC: GCTGTGTTGGAAACGGAGTTG, CTTGCCATGTGGGTTCTGACT
4. CTGF: GTGCCAGAACGCACACTG, CCCCGGTTACACTCCAAA
5. Col1α2: TGCTGCTTGCAGTAACGTCG, TCAACACCATCTCTGCCTCG
6. Fibrosin-I: CACTAAGCCAGAGGCCAAAGTG, ACCAGGAAGGGAATTATAGGGAGG

3.2.9) Statistical analysis

A two-way analysis of variance (ANOVA) or Student's t-test was performed on all quantitative data to determine the change in quantity and statistical significance. Average values were expressed in conjunction with their standard error to reflect their deviation from the true population value. Either Excel or GraphPad Prism was used to generate the graphs while statistical analysis was carried out in GraphPad Prism. The calculated *p*-values were presented in the figures.

3.3) Results

3.3.1) Characterization of decellularized skin

3.3.1.1) Biochemical assays

Our first set of experiments summarized the characterization of decellularized skin. We first measured DNA content in both untreated and treated skin from three different genotypic skin models, wild type, fibrotic skin, and treated fibrotic skin. As seen in Fig. 15, DNA content of WT skin was significantly reduced from 5.57 ±

0.94μg/mg dry weight in non-decellularized skin to 0.27 ± 0.07μg/mg dry weight in decellularized skin ($p < 0.0001$). For fibrotic skin, DNA content was decreased from 3.78 ± 0.86μg/mg dry weight in non-decellularized skin to 0.28 ± 0.03μg/mg dry weight in decellularized skin ($p < 0.001$). For treated fibrotic skin, DNA content also went from 4.26 ± 2.11μg/mg dry weight in control skin to 0.19 ± 0.07μg/mg dry weight in decellularized skin ($p < 0.001$). On average, about 95% of total DNA was removed in three genotypic groups, suggesting that this decellularization method was successful in terms of removing cellular components in the skin.

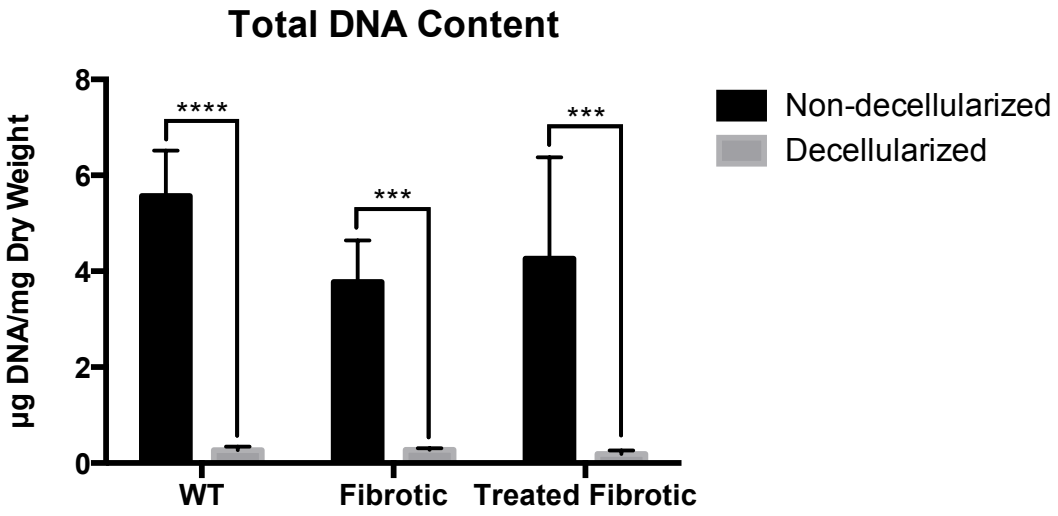

Figure 15. Total DNA content of control and decellularized skin.
Total DNA content was evaluated through the DNA quantification assay and presented as μg of DNA per mg of dry weight for all three groups. Results are shown as the mean of biological replicates +/- standard deviation. ***p < 0.001, ****p < 0.0001.

Next, we quantified one of the major ECM components, collagen, using hydroxyproline assay. Total collagen content in a 5mm biopsy punch was measured in terms of amount of hydroxyproline present in the skin. As seen in Fig. 16, the amount of hydroxyproline remained constant between non-decellularized and decellularized

skin tissues, with 795.62 ± 44.16μg in non-decellularized WT skin and 818.09 ± 22.03μg in decellularized skin, 944.92 ± 50.83μg in non-decellularized fibrotic skin and 1026.08 ± 38.35μg in decellularized skin, and 1005.86 ± 86.03μg in non-decellularized treated fibrotic skin and 1024.82 ± 65.68μg in decellularized skin.

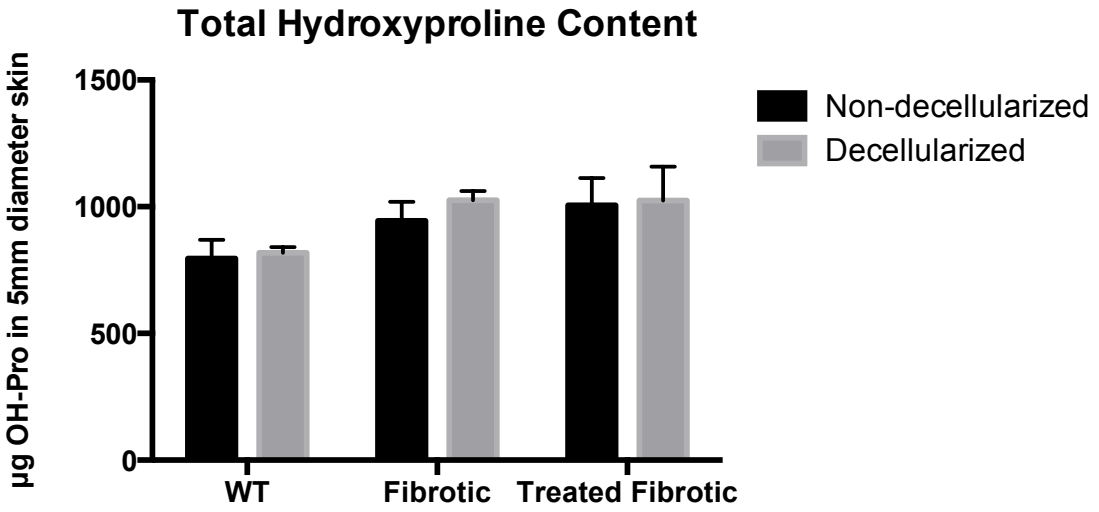

Figure 16. Total hydroxyproline content of control and decellularized skin.
Total collagen content was measured by the hydroxyproline assay and presented as μg of hydroxyproline in a 5mm punch biopsy for all three groups. Results are shown as the mean of biological replicates +/- standard deviation.

We also evaluated total elastin content present in the 5mm biopsy punch of the decellularized tissue as compared to that of the non-decellularized tissue to determine the effect of decellularization on the biochemical composition of ECM in the dermis. As shown in Fig. 17, overall, total elastin content was maintained in all three groups, with 434.49 ± 41.57μg in control WT skin and 468.70 ± 13.91μg in decellularized skin, 710.13 ± 40.82μg in non-decellularized fibrotic skin and 718.67 ± 33.38μg in decellularized skin, and 528.10 ± 36.71μg in control treated fibrotic skin and 542.20 ± 30.15μg in decellularized skin.

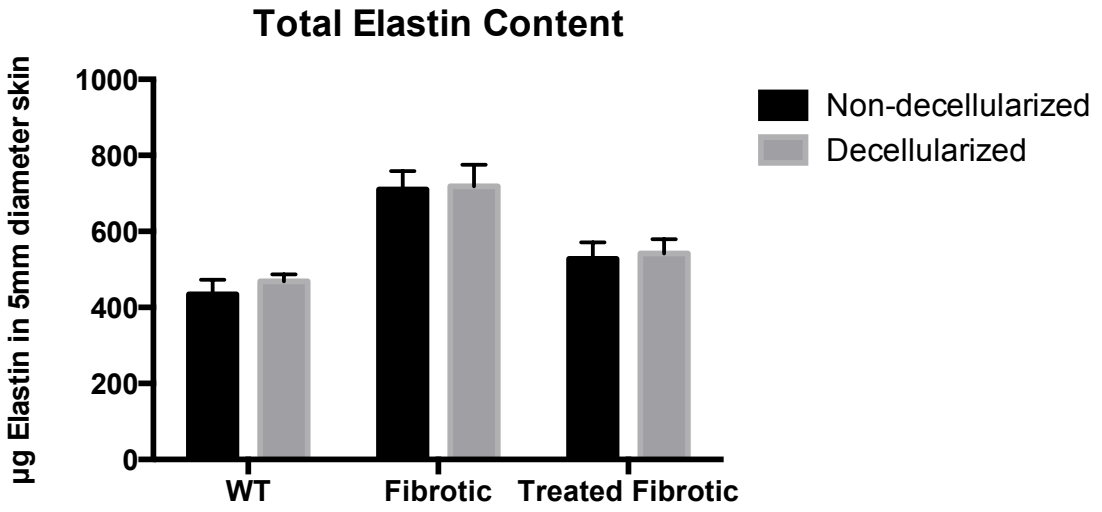

Figure 17. Total elastin content of control and decellularized skin.
Total elastin content was quantified through the Biocolor's Fastin Elastin Assay and presented as μg of elastin in a 5mm punch biopsy fro all three groups. Results are shown as the mean of biological replicates +/- standard deviation.

Another ECM component that we investigated is GAG. GAG quantification of WT skin only was performed through DMMB assay. As seen in Fig. 18, total GAG content was decreased from 7.37 ± 1.42μg per dry weight in non-decellularized skin and 1.50 ± 0.14μg per dry weight in decellularized skin ($p < 0.0001$). The decellularization method used here tends to decrease the amount of GAG present in the skin.

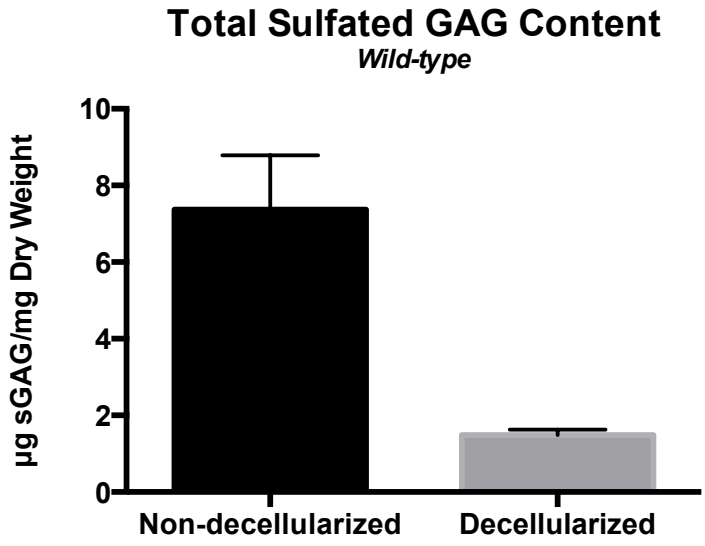

Figure 18. Total GAG content of control and decellularized skin.
Total GAG content was quantified through DMMB assay and presented as μg of DNA per mg of dry weight for WT skin only. Results are represented as the mean of biological replicates +/- standard deviation.

3.3.1.2) Histology

To further validate that the decellularization method has taken effect, hematoxylin and eosin staining was performed on cryo-sectioned samples to visualize the cross-section of skin tissues both before and after decellularization. As shown in Fig. 19, there was a large number of cell nuclei present in the skin, localized in both epidermis and dermis, before decellularization. After the treatment, majority of the cells were removed successfully while leaving the extracellular matrix mostly intact. Overall, the histology well corroborated the biochemical assay data shown before.

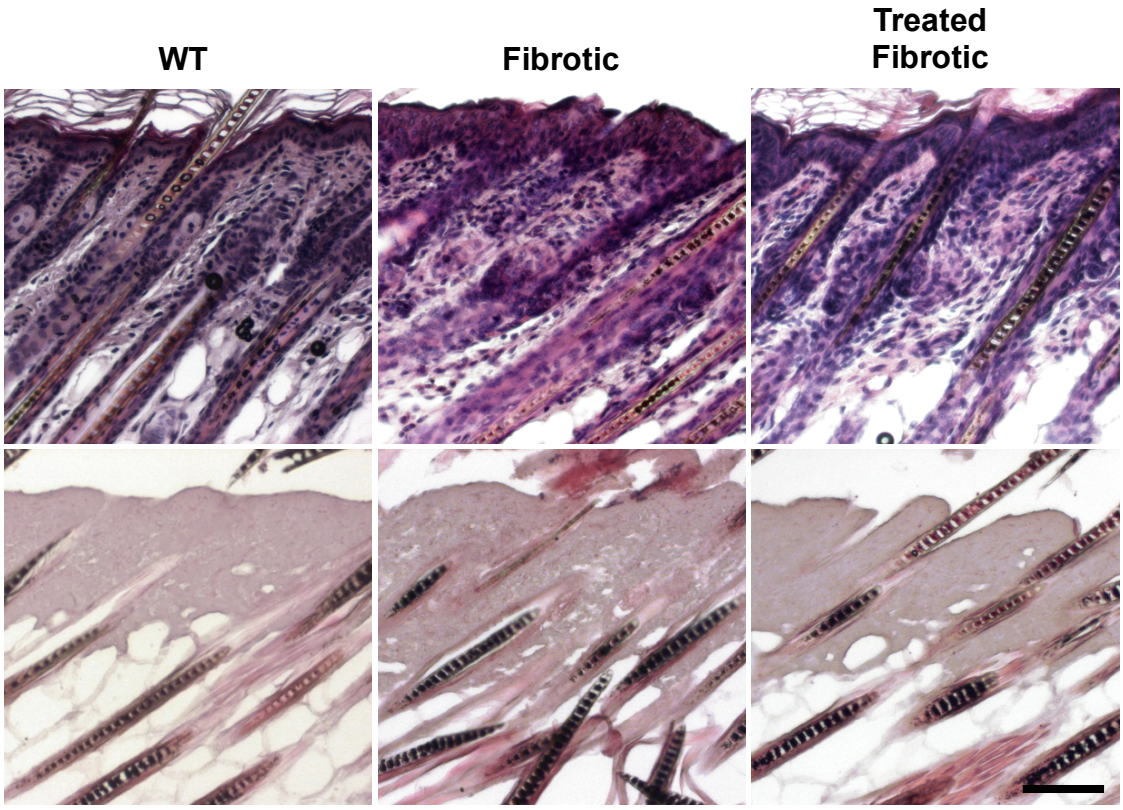

Figure 19. Removal of cells after decellularizing the skin.
Hematoxylin and eosin staining was performed on the three different groups. Top figures represent cross-sections of skin before decellularization. Bottom figures represent cross-sections of skin after the treatment. Scale bar = 100μm.

3.3.2) Cell-matrix interaction

3.3.2.1) qRT-PCR

In the next part of this study, we explored whether the treated fibrotic skin has an effect on transcription levels of genes relevant to fibrosis. Primary dermal fibroblasts were cultured on decellularized WT skin, decellularized fibrotic skin, and decellularized treated fibrotic skin. Cells were collected for RNA extraction and qRT-PCR analysis either on Day 3 or Day 7. Five representative genes associated with fibrotic events were analyzed (Fig. 20). At Day 3, all of the target genes showed

similar expression level in fibrotic and treated fibrotic skin as compared WT skin, but not much variation was found between fibrotic skin and treated fibrotic skin. At Day 7, a similar trend was observed among three genotypic groups. CTGF and Fibrosin I showed similar expression on Day 7 as compared with Day 3. αSMA, SPARC, and Collagen I demonstrated an up-regulation on Day 7 in all matrices compared to day 3. Among five fibrosis-related genes, only Collagen I showed a significant up-regulation in fibrotic skin as compared to WT skin and down-regulation in treated fibrotic skin as compared to Snail transgenic skin although the expression level wasn't brought down as close as to tat of WT skin. One possibility for this observation may be attributed to the loss of some biochemical cues, such as certain cell-secreted factors, in the decellularized skin. Another possibility could be attributed to the 2D culture system in this study. Although fibroblasts were adhered to the surface of the dermis, they did not penetrate into the ECM, experiencing the environment as they would in a biological system. Ultimately, a 3D culturing system may be required for future studies to observe the true changes in the gene expression level.

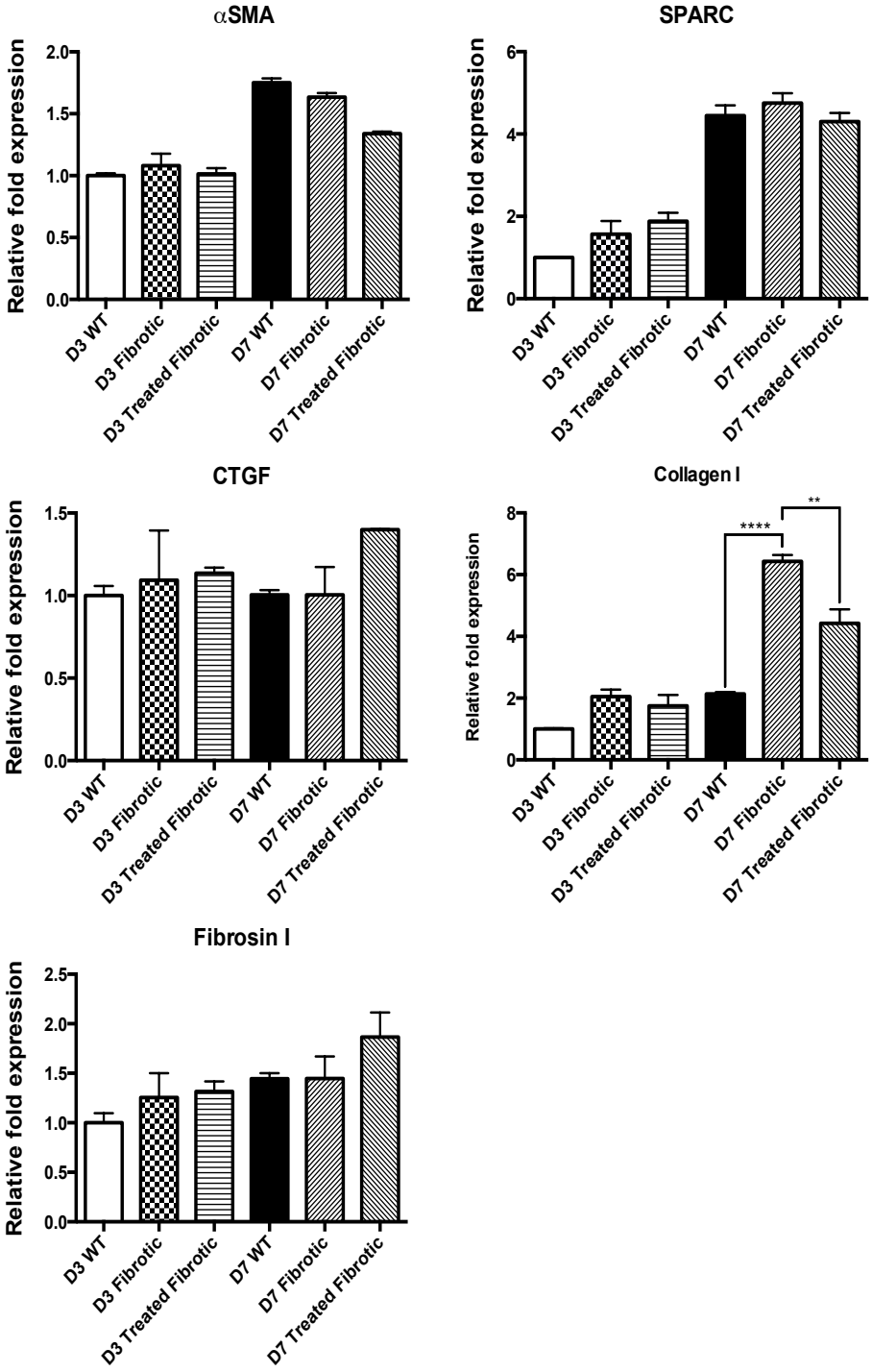

Figure 20. qRT-PCR analysis on decellularized skin with dermal fibroblasts.
qRT-PCR was run on decellularized skin either 3 or 5 days after culturing dermal fibroblasts on it. Results are shown as a mean of biological replicates +/- standard deviation. **$p < 0.01$, ****$p < 0.0001$.

3.4) Discussion

In the first part of this study, we developed a decellularization method for generating a biological scaffold that contains with skin ECM only. Decellularization has been well established to provide biological scaffold matrix in the human clinical studies and animal pre-clinical studies [102]. Protocols of decellularization may vary from physical method, chemical method, enzymatic method to use of protease inhibitors [103]. In our decellularization method, we combined the use of hypotonic and hypertonic solutions with enzymatic treatment to fully remove the cellular components from the tissues. This method successfully removed cellular components without altering the ECM structure. Through DNA quantification and H&E staining, we both quantitatively and visually ensured that majority of the cells were removed from the epidermis and dermis with only a small trace of DNA fragments. Collagen and elastin contents were unchanged during the process as shown in the hydroxyproline and elastin assays. However, a major reduction in the GAG content of the decellularized skin was observed. This could partly due to the removal of GAGs associated with cell membrane as studies have shown that about 30% of GAGs is typically on the cell membrane [104]. In addition, the incubation in salt solution used here may possibly disrupt the electrostatic forces that contribute to ECM assembly, thereby leaching out GAG. Other studies have also shown a certain degree of GAG loss during decellularization [105, 106].

In the second part of this study, by culturing primary dermal fibroblasts for three or seven days, we investigated the gene expression associated with fibroblast

activation from the extracted RNA of cultured cells. A number of studies have demonstrated that activated fibroblasts are one of the key mediators in a variety of tissue fibrosis [27, 33, 34, 50]. Also, activated fibroblasts has been shown to have up-regulation in genes like α-SMA, SPARC, CTGF, Collagen I, and Fibrosin I [33]. In our study, we only observed an up-regulation in Collagen I of fibrotic skin, implying a possible activation occurring in the cultured fibroblasts. All other genes showed no significant up-regulation at the two specific time points. In treated fibrotic skin, we were able to observe a down-regulation of Collagen I, suggesting the effect of elastic fibers in activation of fibroblasts. The culture system used in this study is 2D, which implies that the cells are only on the surface of the matrix. This may also prevent the cells from fully experiencing the environment. Although there are some limitations in the study, the data we present provides some preliminary evidence for the impact of physical properties of skin on activation of fibroblasts.

3.5) Future studies

This study demonstrates the effect of ECM in fibrosis progression of skin. Through the decellularization process, we were able to obtain a decellularized skin matrix with complete removal of host cells while maintaining the major ECM components of interest, collagen and elastin. We also evaluated the expression level of genes associated with fibroblast activation to investigate how different physical properties may affect the activation of resident fibroblasts. For future studies, a 3D culturing model system should be established to provide cells with an environment that more closely mimics the biological dermis of skin.

3.6) Acknowledgement

Chapter 3, in part, will be prepared for submission for publication of the material: Nakasaki, Manando; Hwang, Yongsung; Xie, Yun; Varghese, Shyni; Jamora, Colin. The thesis author will be the co-author of this paper.

REFERENCES

1. Frantz, C., K.M. Stewart, and V.M. Weaver, *The extracellular matrix at a glance.* J Cell Sci, 2010. **123**(Pt 24): p. 4195-200.

2. Rozario, T. and D.W. DeSimone, *The extracellular matrix in development and morphogenesis: a dynamic view.* Dev Biol, 2010. **341**(1): p. 126-40.

3. Daley, W.P., S.B. Peters, and M. Larsen, *Extracellular matrix dynamics in development and regenerative medicine.* Journal of cell science, 2008. **121**(3): p. 255-264.

4. Ricard-Blum, S., *The collagen family.* Cold Spring Harb Perspect Biol, 2011. **3**(1): p. a004978.

5. Gordon, M.K. and R.A. Hahn, *Collagens.* Cell and tissue research, 2010. **339**(1): p. 247-257.

6. Kielty, C.M., *Elastic fibres in health and disease.* Expert Rev Mol Med, 2006. **8**(19): p. 1-23.

7. Smith, M.L., et al., *Force-induced unfolding of fibronectin in the extracellular matrix of living cells.* PLoS Biol, 2007. **5**(10): p. e268.

8. Grinnell, F., *Fibronectin and wound healing.* J Cell Biochem, 1984. **26**(2): p. 107-16.

9. Iozzo, R.V. and A.D. Murdoch, *Proteoglycans of the extracellular environment: clues from the gene and protein side offer novel perspectives in molecular diversity and function.* FASEB J, 1996. **10**(5): p. 598-614.

10. Schaefer, L. and R.M. Schaefer, *Proteoglycans: from structural compounds to signaling molecules.* Cell and tissue research, 2010. **339**(1): p. 237-246.

11. Iozzo, R.V., *The biology of the small leucine-rich proteoglycans. Functional network of interactive proteins.* J Biol Chem, 1999. **274**(27): p. 18843-6.

12. Bosman, F.T. and I. Stamenkovic, *Functional structure and composition of the extracellular matrix.* J Pathol, 2003. **200**(4): p. 423-8.

13. Hynes, R.O., *The extracellular matrix: not just pretty fibrils.* Science, 2009. **326**(5957): p. 1216-1219.

14. Schultz, G.S. and A. Wysocki, *Interactions between extracellular matrix and growth factors in wound healing.* Wound Repair and Regeneration, 2009. **17**(2): p. 153-162.

15. Brack, A.S., et al., *Increased Wnt signaling during aging alters muscle stem cell fate and increases fibrosis.* Science, 2007. **317**(5839): p. 807-810.

16. Conboy, I.M., et al., *Rejuvenation of aged progenitor cells by exposure to a young systemic environment.* Nature, 2005. **433**(7027): p. 760-764.

17. Wynn, T.A. and T.R. Ramalingam, *Mechanisms of fibrosis: therapeutic translation for fibrotic disease.* Nat Med, 2012. **18**(7): p. 1028-40.

18. Wynn, T.A., *Common and unique mechanisms regulate fibrosis in various fibroproliferative diseases.* J Clin Invest, 2007. **117**(3): p. 524-9.

19. Verrecchia, F. and A. Mauviel, *Transforming growth factor-beta and fibrosis.* World Journal of Gastroenterology, 2007. **13**(22): p. 3056-62.

20. Wynn, T.A., *IL-13 effector functions*.* Annual review of immunology, 2003. **21**(1): p. 425-456.

21. Mutsaers, S.E., et al., *Mechanisms of tissue repair: from wound healing to fibrosis.* The international journal of biochemistry & cell biology, 1997. **29**(1): p. 5-17.

22. Zeisberg, M. and R. Kalluri, *Cellular mechanisms of tissue fibrosis. 1. Common and organ-specific mechanisms associated with tissue fibrosis.* Am J Physiol Cell Physiol, 2013. **304**(3): p. C216-25.

23. Trojanowska, M., et al., *Pathogenesis of fibrosis: type 1 collagen and the skin.* J Mol Med (Berl), 1998. **76**(3-4): p. 266-74.

24. Jinnin, M., *Mechanisms of skin fibrosis in systemic sclerosis.* J Dermatol, 2010. **37**(1): p. 11-25.

25. Bataller, R. and D.A. Brenner, *Liver fibrosis.* J Clin Invest, 2005. **115**(2): p. 209-18.

26. Czubryt, M.P., *Common threads in cardiac fibrosis, infarct scar formation, and wound healing.* Fibrogenesis Tissue Repair, 2012. **5**(1): p. 19.

27. Davis, J. and J.D. Molkentin, *Myofibroblasts: Trust your heart and let fate decide.* J Mol Cell Cardiol, 2013.

28. Baud, L., B. Fouqueray, and A. Bellocq, *Inflammatory mechanisms of renal fibrosis: glomerulonephritis.* Bull Acad Natl Med, 1999. **183**(1): p. 23-31.

29. Crouch, E., *Pathobiology of pulmonary fibrosis.* American Journal of Physiology-Lung Cellular and Molecular Physiology, 1990. **259**(4): p. L159-L184.

30. Mann, C.J., et al., *Aberrant repair and fibrosis development in skeletal muscle.* Skelet Muscle, 2011. **1**(1): p. 21.

31. Serrano, A.L. and P. Munoz-Canoves, *Regulation and dysregulation of fibrosis in skeletal muscle.* Exp Cell Res, 2010. **316**(18): p. 3050-8.

32. Wynn, T.A., *Cellular and molecular mechanisms of fibrosis.* J Pathol, 2008. **214**(2): p. 199-210.

33. Klingberg, F., B. Hinz, and E.S. White, *The myofibroblast matrix: implications for tissue repair and fibrosis.* J Pathol, 2013. **229**(2): p. 298-309.

34. Krieg, T., D. Abraham, and R. Lafyatis, *Fibrosis in connective tissue disease: the role of the myofibroblast and fibroblast-epithelial cell interactions.* Arthritis Research and Therapy, 2007. **9**(2): p. S4.

35. Kalluri, R. and E.G. Neilson, *Epithelial-mesenchymal transition and its implications for fibrosis.* Journal of Clinical Investigation, 2003. **112**(12): p. 1776-1784.

36. Piera-Velazquez, S., Z. Li, and S.A. Jimenez, *Role of endothelial-mesenchymal transition (EndoMT) in the pathogenesis of fibrotic disorders.* The American journal of pathology, 2011. **179**(3): p. 1074-1080.

37. Willis, B.C., R.M. duBois, and Z. Borok, *Epithelial origin of myofibroblasts during fibrosis in the lung.* Proc Am Thorac Soc, 2006. **3**(4): p. 377-82.

38. Bucala, R., et al., *Circulating fibrocytes define a new leukocyte subpopulation that mediates tissue repair.* Mol Med, 1994. **1**(1): p. 71-81.

39. Quan, T.E., S.E. Cowper, and R. Bucala, *The role of circulating fibrocytes in fibrosis.* Curr Rheumatol Rep, 2006. **8**(2): p. 145-50.

40. Lin, S.L., et al., *Pericytes and perivascular fibroblasts are the primary source of collagen-producing cells in obstructive fibrosis of the kidney.* Am J Pathol, 2008. **173**(6): p. 1617-27.

41. O'Reilly, S., *Role of interleukin-13 in fibrosis, particularly systemic sclerosis.* Biofactors, 2013.

42. Wynn, T.A., *Fibrotic disease and the T(H)1/T(H)2 paradigm.* Nat Rev Immunol, 2004. **4**(8): p. 583-94.

43. Lee, C.G., et al., *Interleukin-13 induces tissue fibrosis by selectively stimulating and activating transforming growth factor beta(1).* J Exp Med, 2001. **194**(6): p. 809-21.

44. Kaviratne, M., et al., *IL-13 activates a mechanism of tissue fibrosis that is completely TGF-beta independent.* J Immunol, 2004. **173**(6): p. 4020-9.

45. Leask, A. and D.J. Abraham, *TGF-beta signaling and the fibrotic response.* FASEB J, 2004. **18**(7): p. 816-27.

46. Bonner, J.C., *Regulation of PDGF and its receptors in fibrotic diseases.* Cytokine Growth Factor Rev, 2004. **15**(4): p. 255-73.

47. Igarashi, A., et al., *Connective tissue growth factor gene expression in tissue sections from localized scleroderma, keloid, and other fibrotic skin disorders.* J Invest Dermatol, 1996. **106**(4): p. 729-33.

48. Leask, A., C.P. Denton, and D.J. Abraham, *Insights into the molecular mechanism of chronic fibrosis: the role of connective tissue growth factor in scleroderma.* J Invest Dermatol, 2004. **122**(1): p. 1-6.

49. Hinz, B., *Tissue stiffness, latent TGF-β1 activation, and mechanical signal transduction: implications for the pathogenesis and treatment of fibrosis.* Current rheumatology reports, 2009. **11**(2): p. 120-126.

50. Wipff, P.J., et al., *Myofibroblast contraction activates latent TGF-beta1 from the extracellular matrix.* J Cell Biol, 2007. **179**(6): p. 1311-23.

51. Velleman, S.G., *The role of the extracellular matrix in skeletal muscle development.* Poultry science, 1999. **78**(5): p. 778-784.

52. Gillies, A.R. and R.L. Lieber, *Structure and function of the skeletal muscle extracellular matrix.* Muscle Nerve, 2011. **44**(3): p. 318-31.

53. Kjaer, M., *Role of extracellular matrix in adaptation of tendon and skeletal muscle to mechanical loading.* Physiol Rev, 2004. **84**(2): p. 649-98.

54. Gosselin, L.E., *Skeletal Muscle Collagen: Age, Injury and Disease*, in *Sarcopenia–Age-Related Muscle Wasting and Weakness*. 2011, Springer. p. 159-172.

55. Brandan, E., C. Cabello-Verrugio, and C. Vial, *Novel regulatory mechanisms for the proteoglycans decorin and biglycan during muscle formation and muscular dystrophy.* Matrix Biol, 2008. **27**(8): p. 700-8.

56. Brandan, E. and J. Gutierrez, *Role of skeletal muscle proteoglycans during myogenesis.* Matrix Biology, 2013.

57. Conboy, I.M. and T.A. Rando, *Aging, stem cells and tissue regeneration: lessons from muscle.* Cell cycle, 2005. **4**(3): p. 407-410.

58. Jenniskens, G.J., J.H. Veerkamp, and T.H. van Kuppevelt, *Heparan sulfates in skeletal muscle development and physiology.* J Cell Physiol, 2006. **206**(2): p. 283-94.

59. Li, Y., et al., *Transforming growth factor-beta1 induces the differentiation of myogenic cells into fibrotic cells in injured skeletal muscle: a key event in muscle fibrogenesis.* Am J Pathol, 2004. **164**(3): p. 1007-19.

60. Kragstrup, T.W., M. Kjaer, and A.L. Mackey, *Structural, biochemical, cellular, and functional changes in skeletal muscle extracellular matrix with aging.* Scand J Med Sci Sports, 2011. **21**(6): p. 749-57.

61. Ryall, J.G., J.D. Schertzer, and G.S. Lynch, *Cellular and molecular mechanisms underlying age-related skeletal muscle wasting and weakness.* Biogerontology, 2008. **9**(4): p. 213-28.

62. Conboy, I.M., et al., *Notch-mediated restoration of regenerative potential to aged muscle.* Science, 2003. **302**(5650): p. 1575-7.

63. Carlson, B.M., et al., *Skeletal muscle regeneration in very old rats.* The Journals of Gerontology Series A: Biological Sciences and Medical Sciences, 2001. **56**(5): p. B224-B233.

64. Bonilla, E., et al., *Duchenne muscular dystrophy: deficiency of dystrophin at the muscle cell surface.* Cell, 1988. **54**(4): p. 447-452.

65. Deconinck, N. and B. Dan, *Pathophysiology of duchenne muscular dystrophy: current hypotheses.* Pediatr Neurol, 2007. **36**(1): p. 1-7.

66. Porter, J.D., et al., *A chronic inflammatory response dominates the skeletal muscle molecular signature in dystrophin-deficient mdx mice.* Hum Mol Genet, 2002. **11**(3): p. 263-72.

67. Goldspink, G., et al., *Age-related changes in collagen gene expression in the muscles of mdx dystrophic and normal mice.* Neuromuscular Disorders, 1994. **4**(3): p. 183-191.

68. Marshall, P., P. Williams, and G. Goldspink, *Accumulation of collagen and altered fiber□type ratios as indicators of abnormal muscle gene expression in the mdx dystrophic mouse.* Muscle & nerve, 1989. **12**(7): p. 528-537.

69. Farndale, R.W., D.J. Buttle, and A.J. Barrett, *Improved quantitation and discrimination of sulphated glycosaminoglycans by use of dimethylmethylene blue.* Biochim Biophys Acta, 1986. **883**(2): p. 173-7.

70. Faulkner, J.A., et al., *Age-related changes in the structure and function of skeletal muscles.* Clinical and Experimental Pharmacology and Physiology, 2007. **34**(11): p. 1091-1096.

71. Pastoret, C. and A. Sebille, *Further aspects of muscular dystrophy in mdx mice.* Neuromuscular Disorders, 1993. **3**(5): p. 471-475.

72. Alnaqeeb, M.A., N.S. Al Zaid, and G. Goldspink, *Connective tissue changes and physical properties of developing and ageing skeletal muscle.* J Anat, 1984. **139 (Pt 4)**: p. 677-89.

73. Mohan, S. and E. Radha, *Age-related changes in rat muscle collagen.* Gerontology, 1980. **26**(2): p. 61-7.

74. Vidal, B., et al., *Fibrinogen drives dystrophic muscle fibrosis via a TGFβ/alternative macrophage activation pathway.* Genes & development, 2008. **22**(13): p. 1747-1752.

75. Duance, V., et al., *A role for collagen in the pathogenesis of muscular dystrophy?* 1980.

76. Bernfield, M., et al., *Functions of cell surface heparan sulfate proteoglycans.* Annu Rev Biochem, 1999. **68**: p. 729-77.

77. Carey, D.J., *Syndecans: multifunctional cell-surface co-receptors.* Biochem J, 1997. **327 (Pt 1)**: p. 1-16.

78. Ruoslahti, E. and Y. Yamaguchi, *Proteoglycans as modulators of growth factor activities.* Cell, 1991. **64**(5): p. 867-9.

79. Brandan, E., M.E. Fuentes, and W. Andrade, *The proteoglycan decorin is synthesized and secreted by differentiated myotubes.* Eur J Cell Biol, 1991. **55**(2): p. 209-16.

80. Carrino, D.A., J.M. Sorrell, and A.I. Caplan, *Dynamic expression of proteoglycans during chicken skeletal muscle development and maturation.* Poult Sci, 1999. **78**(5): p. 769-77.

81. WATANABE, K., et al., *Age-related changes in the content and composition of glycosaminoglycans isolated from the mouse skeletal muscle: normal and dystrophic conditions.* Journal of biochemistry, 1986. **100**(1): p. 167-173.

82. Cáceres, S., et al., *Synthesis of proteoglycans is augmented in dystrophic mdx mouse skeletal muscle.* European journal of cell biology, 2000. **79**(3): p. 173-181.

83. Maxwell, L.C., J.A. Faulkner, and G.J. Hyatt, *Estimation of number of fibers in guinea pig skeletal muscles.* J Appl Physiol, 1974. **37**(2): p. 259-64.

84. Rogers, M.A. and W.J. Evans, *Changes in skeletal muscle with aging: effects of exercise training.* Exerc Sport Sci Rev, 1993. **21**: p. 65-102.

85. Sato, T., et al., *Age changes in size and number of muscle fibers in human minor pectoral muscle.* Mech Ageing Dev, 1984. **28**(1): p. 99-109.

86. Alnaqeeb, M. and G. Goldspink, *Changes in fibre type, number and diameter in developing and ageing skeletal muscle.* Journal of anatomy, 1987. **153**: p. 31.

87. Lexell, J., C.C. Taylor, and M. Sjostrom, *What is the cause of the ageing atrophy? Total number, size and proportion of different fiber types studied in whole vastus lateralis muscle from 15- to 83-year-old men.* J Neurol Sci, 1988. **84**(2-3): p. 275-94.

88. Daw, C.K., J.W. Starnes, and T.P. White, *Muscle atrophy and hypoplasia with aging: impact of training and food restriction.* J Appl Physiol (1985), 1988. **64**(6): p. 2428-32.

89. Sheard, P.W. and R.D. Anderson, *Age-related loss of muscle fibres is highly variable amongst mouse skeletal muscles.* Biogerontology, 2012. **13**(2): p. 157-67.

90. Renault, V., et al., *Regenerative potential of human skeletal muscle during aging.* Aging cell, 2002. **1**(2): p. 132-139.

91. Barazzoni, R., K.R. Short, and K.S. Nair, *Effects of aging on mitochondrial DNA copy number and cytochrome c oxidase gene expression in rat skeletal muscle, liver, and heart.* J Biol Chem, 2000. **275**(5): p. 3343-7.

92. Kottlors, M. and J. Kirschner, *Elevated satellite cell number in Duchenne muscular dystrophy.* Cell and tissue research, 2010. **340**(3): p. 541-548.

93. Brack, A.S., H. Bildsoe, and S.M. Hughes, *Evidence that satellite cell decrement contributes to preferential decline in nuclear number from large fibres during murine age-related muscle atrophy.* J Cell Sci, 2005. **118**(Pt 20): p. 4813-21.

94. Haake, A., G.A. Scott, and K.A. Holbrook, *Structure and function of the skin: overview of the epidermis and dermis.* The Biology of the skin, 2001. **2001**: p. 19-45.

95. Proksch, E., J.M. Brandner, and J.M. Jensen, *The skin: an indispensable barrier.* Exp Dermatol, 2008. **17**(12): p. 1063-72.

96. Du, F., et al., *Expression of snail in epidermal keratinocytes promotes cutaneous inflammation and hyperplasia conducive to tumor formation.* Cancer Res, 2010. **70**(24): p. 10080-9.

97. Cano, A., et al., *The transcription factor snail controls epithelial–mesenchymal transitions by repressing E-cadherin expression.* Nature cell biology, 2000. **2**(2): p. 76-83.

98. Boutet, A., et al., *Snail activation disrupts tissue homeostasis and induces fibrosis in the adult kidney.* The EMBO journal, 2006. **25**(23): p. 5603-5613.

99. Jamora, C., et al., *A signaling pathway involving TGF-beta2 and snail in hair follicle morphogenesis.* PLoS Biol, 2005. **3**(1): p. e11.

100. Jamora, C., et al., *A signaling pathway involving TGF-β2 and snail in hair follicle morphogenesis.* PLoS biology, 2004. **3**(1): p. e11.

101. Livak, K.J. and T.D. Schmittgen, *Analysis of relative gene expression data using real-time quantitative PCR and the 2(-Delta Delta C(T)) Method.* Methods, 2001. **25**(4): p. 402-8.

102. Badylak, S.F., D. Taylor, and K. Uygun, *Whole-organ tissue engineering: decellularization and recellularization of three-dimensional matrix scaffolds.* Annu Rev Biomed Eng, 2011. **13**: p. 27-53.

103. Gilbert, T.W., T.L. Sellaro, and S.F. Badylak, *Decellularization of tissues and organs.* Biomaterials, 2006. **27**(19): p. 3675-83.

104. Mertens, G., et al., *Cell surface heparan sulfate proteoglycans from human vascular endothelial cells. Core protein characterization and antithrombin III binding properties.* J Biol Chem, 1992. **267**(28): p. 20435-43.

105. Bondioli, E., et al., *Development and evaluation of a decellularized membrane from human dermis.* J Tissue Eng Regen Med, 2012.

106. Choi, Y.C., et al., *Decellularized extracellular matrix derived from porcine adipose tissue as a xenogeneic biomaterial for tissue engineering.* Tissue Eng Part C Methods, 2012. **18**(11): p. 866-76.